Practical sand transport formula for non-breaking waves and currents

Dominic A. van der A[a,*], Jan S. Ribberink[b], Jebbe J. van der Werf[b,c], Tom O'Donoghue[a], René H. Buijsrogge[b] and Wouter M. Kranenburg[b]

[a] University of Aberdeen, School of Engineering, King's College, Aberdeen, AB24 3UE, United Kingdom
[b] Water Engineering and Management, University of Twente, P.O. Box 217, 7500 AE, Enschede, The Netherlands
[c] Marine and Coastal Systems, Deltares, P.O. Box 177, 2600 MH, Delft, The Netherlands

ABSTRACT

Many existing practical sand transport formulae for the coastal marine environment are restricted to a limited range of hydrodynamic and sand conditions. This paper presents a new practical formula for net sand transport induced by non-breaking waves and currents. The formula is especially developed for cross-shore sand transport under wave-dominated conditions and is based on the semi-unsteady, half wave-cycle concept, with bed shear stress as the main forcing parameter. Unsteady phase-lag effects between velocities and concentrations, which are especially important for rippled bed and fine sand sheet-flow conditions, are accounted for through parameterisations. Recently-recognized effects on the net transport rate related to flow acceleration skewness and progressive surface waves are also included. To account for the latter, the formula includes the effects of boundary layer streaming and advection effects which occur under real waves, but not in oscillatory tunnel flows. The formula is developed using a database of 226 net transport rate measurements from large-scale oscillatory flow tunnels and a large wave flume, covering a wide range of full-scale flow conditions and uniform and graded sands with median diameter ranging from 0.13mm to 0.54mm. Good overall agreement is obtained between observed and predicted net transport rates with 78% of the predictions falling within a factor 2 of the measurements. For several distinctly different conditions, the behaviour of the net transport with increasing flow strength agrees well with observations, indicating that the most important transport processes in both the rippled bed and sheet flow regime are well captured by the formula. However, for some flow conditions

* Corresponding author. Tel.: +44 1224 272806; fax.: +44 1224 272497.
Email address: d.a.vandera@abdn.ac.uk (D.A. van der A)

good quantitative agreement could only be obtained by introducing separate calibration parameters. The new formula has been validated against independent net transport rate data for oscillatory flow conditions and steady flow conditions.

KEYWORDS: sediment transport formula, sheet flow, ripples, bed shear stress, phase lag effects, advection effects

1.0 INTRODUCTION

In recent years a substantial body of field- and laboratory-based research has been devoted to measuring sand transport processes induced by waves and currents, and predictive approaches for the net, wave-averaged sand transport have been developed. Generally, these approaches can be classified as process-based numerical models or parameterised (engineering) formulae. Process-based models represent many of the detailed physical processes involved in sand transport by waves and currents, and resolve the vertical and sometimes also the horizontal structure of the time-dependent, intra-wave velocity and sand concentration fields. Such models (see e.g. Hendersen et al., 2004; Holmedal et al., 2009; Hassan and Ribberink, 2010) are often restricted to specific flow and sand conditions, require relatively long computation times and are therefore generally not implemented in coastal morphodynamic models. Parameterised sand transport formulae on the other hand, consist of a set of relatively simple equations often covering a wide range of flow and sand conditions, require short computation times and can be implemented easily in coastal morphodynamic models.

Practical sand transport formulae for the coastal marine environment are generally semi-empirical formulae which can be classified as time-averaged, quasi-steady or semi-unsteady. Based on approaches used for fluvial sediment transport, time-averaged formulae predict sand transport at a timescale that is much longer than the wave period, using wave-averaged values of velocity and sand concentration. The Bijker (1971) formula is an example of a widely-used time-averaged transport formula, in which waves act as stirring agent for the current-related

transport (suspended load and bed load). In time-averaged formulae, the total net transport is always in the direction of the mean current and the wave-related transport component is not taken into account.

Quasi-steady formulae calculate intra-wave sand transport, with the assumption that the instantaneous sand transport relates only to the instantaneous forcing parameter, either the flow velocity or bed shear stress. Commonly-used quasi-steady formulae predict non-zero net transport resulting from velocity skewness, as occurs under Stokes-type waves (e.g. Bailard, 1981; Ribberink, 1998; Soulsby and Damgaard, 2005; Wang, 2007), but most do not account for transport resulting from acceleration skewness, as occurs under sawtooth-shaped waves (Watanabe and Sato, 2004; Van der A et al., 2010). Formulae that do account for both velocity and acceleration skewness have mostly been developed for sheet-flow conditions (e.g. Nielsen, 2006; Gonzalez-Rodriguez and Madsen, 2007; Suntoyo et al., 2008) and do not apply to lower energy conditions when the bed is generally covered with ripples.

The assumption of quasi-steadiness only holds for conditions for which the reaction time of sand particles is short relative to the wave period. In other words, the pick-up and settling of sand particles must take place in a much shorter time than the wave period. This assumption is not the case for fine sand sheet-flow conditions (Dohmen-Janssen et al., 2002; O'Donoghue and Wright, 2004; Van der A et al., 2009) and rippled bed conditions (Van der Werf et al., 2007), where phase lag effects can significantly affect the magnitude and sometimes even the direction of the net transport rate. Semi-unsteady formulae have been developed to account for phase lag effects in sheet-flow conditions (Dibajnia and Watanabe, 1992; Camenen and Larson, 2007), rippled bed conditions (Nielsen, 1988; Van der Werf et al., 2006) and for both sheet-flow and ripple conditions (Silva et al., 2006; Van Rijn, 2007a,b,c).

Existing transport formulae are based for the most part on experimental data from oscillatory flow tunnels, in which the flow is horizontal and horizontally uniform. However, net transport

rate experiments carried out in large wave flumes (Ribberink et al., 2000; Dohmen-Janssen and Hanes, 2002; Schretlen et al., 2011) indicate that the added complexities in the hydrodynamics of surface waves compared to tunnel flows can be important in determining the net sand transport. Kranenburg et al. (in press) use a detailed advection-diffusion boundary layer sand transport model and the above mentioned tunnel and flume data to quantify the importance of progressive wave, streaming-related, bed shear stress (wave Reynolds stress) and, at least for fine sand, of vertical advection of sand by vertical orbital velocities and horizontal advection of sand by gradients in the horizontal sediment flux. Existing transport models do not account for these real wave effects, although Nielsen (2006) does incorporate a streaming-related bed shear stress in his formulation, while Van Rijn (2007a) incorporates streaming by adding a small steady current at the edge of the wave boundary layer. Nielsen (2006) has shown that the net transport of medium sand is better predicted when a streaming-related mean bed shear stress is added to the instantaneous oscillatory bed shear stress in a 'quasi-steady' Meyer-Peter and Müller type sand transport formula.

This paper presents a new semi-unsteady formula for predicting net sand transport under waves and currents. Based on an extensive dataset of measurements of net sand transport rates from large-scale laboratory experiments, covering a wide range of hydraulic conditions and transport regimes, the formula can be applied to rippled bed and sheet-flow conditions, incorporates phase lag and flow acceleration effects, and can be applied to both oscillatory flow and surface wave conditions. The new sand transport formula is presented in Section 2.0 of the paper. Section 3.0 presents a comparison of calculated net transport rates with measured transport rates from the large scale-experiments. The general behaviour of predicted net transport rates across a range of flow conditions is examined in Section 4.0. Section 5.0 presents the results of validation tests against independent data for oscillatory flow and steady flow conditions. A discussion of results and conclusions from the paper are presented in Sections 6.0 and 7.0 respectively.

2.0 SAND TRANSPORT FORMULA FOR OSCILLATORY FLOWS AND PROGRESSIVE WAVES

The new transport formula is based on a modified version of the semi-unsteady "half-cycle" concept originally proposed by Dibajnia and Watanabe (1992). In this concept the wave-averaged total net sand transport rate (bedload and suspended load) as taking place in the oscillatory boundary layer is essentially described as the difference between the two gross amounts of sand transported during the positive "crest" half-cycle and during the negative "trough" half-cycle. Unsteady phase lag effects are taken into account via two contributions to the amount of sand transported during each half-cycle: sand entrained and transported during the present half-cycle and sand entrained during the previous half-cycle which is transported during the present half-cycle; the latter is the phase lag contribution. The present formula differs from Dibajnia and Watanabe (1992) in the following ways: (i) bed shear stress rather than near-bed velocity is used as the main forcing parameter; (ii) the effects of flow unsteadiness (phase lag effects) are incorporated in a different way; (iii) the effects of acceleration skewness are incorporated; (iv) it covers graded sands and (v) the formula distinguishes between oscillatory flows and progressive surface waves. The present formula distinguishes itself from other half-cycle-type formulae (Dibajnia & Watanabe, 1996, 1998; Watanabe and Sato, 2004; Silva et al., 2006) through (v), as well as through the calculation of the detailed sub-processes and the extent of experimental data used to inform formula development and calibration.

In the new formula, the non-dimensional net transport rate is given by the following "velocity-load" equation:

$$\vec{\Phi} = \frac{\vec{q}_s}{\sqrt{(s-1)gd_{50}^3}} = \frac{\sqrt{|\theta_c|}T_c\left(\Omega_{cc} + \frac{T_c}{2T_{cu}}\Omega_{tc}\right)\frac{\vec{\theta}_c}{|\theta_c|} + \sqrt{|\theta_t|}T_t\left(\Omega_{tt} + \frac{T_t}{2T_{tu}}\Omega_{ct}\right)\frac{\vec{\theta}_t}{|\theta_t|}}{T} \quad (1)$$

where $\vec{q}_s$ is the volumetric net transport rate per unit width, $s = (\rho_s - \rho)/\rho$ where ρ_s and ρ are the densities of sand and water respectively, g is acceleration due to gravity and d_{50} is the sand median diameter; $\vec{\theta}$ is the non-dimensional bed shear stress (Shields parameter), with

subscripts “c” and “t” implying “crest” and “trough” half cycle respectively; T is wave period; T_c is the duration of the crest (positive) half cycle and T_{cu} is the duration of accelerating flow within the crest half cycle (Figure 1); similarly T_t is the duration of the trough (negative) half cycle and T_{tu} the period of accelerating flow within the trough half cycle.

There are four contributions to the net sand transport:

- Ω_{cc} represents the sand load that is entrained during the wave crest period and transported during the crest period;
- Ω_{ct} represents the sand load that is entrained during the wave crest period and transported during the trough period;
- Ω_{tt} represents the sand load that is entrained during the wave trough period and transported during the trough period;
- Ω_{tc} represents the sand load that is entrained during the wave trough period and transported during the crest period.

The total sand load in each half-cycle is multiplied by $\sqrt{\theta_i}$ (with subscript “i” either “c” for crest or “t” for trough), representing the non-dimensional friction velocity, to obtain the non-dimensional half-cycle transport rate. Both half-cycle transport rates are weighted with their duration relative to the wave period (T_c/T and T_t/T, respectively). The multipliers $\frac{T_c}{2T_{cu}}$ and $\frac{T_t}{2T_{tu}}$ on Ω_{tc} and Ω_{ct} respectively account for the effect of acceleration skewness on the travel distance of the fraction of sand remaining in suspension after flow reversal, since suspended sand is transported further when followed by a steep front half-wave cycle compared to a gradual front half-wave cycle (Watanabe and Sato, 2004).

The sand load entrained in the flow during each half-cycle is related to the Shields parameter as follows:

$$\Omega_i = \begin{cases} 0 & \text{if } |\theta_i| \le \theta_{cr} \\ m\left(|\theta_i| - \theta_{cr}\right)^n & \text{if } |\theta_i| > \theta_{cr} \end{cases} \tag{2}$$

where the critical Shields number, θ_{cr}, is calculated following Soulsby (1997). The proportionality constant m and power of the excess Shields parameter n are two of the three main calibration coefficients of the transport formula.

Application of Eq. (1) to calculate the net sand transport rate in oscillatory flow or under progressive surface waves requires the following three main steps: (i) establish the "representative" crest half-cycle and trough half-cycle water particle velocities, as well as the representative full-cycle orbital velocity and excursion; (ii) calculate the bed shear stress (Shields parameter) for each flow half cycle; (iii) calculate the sediment load entrained during each flow half-cycle and determine the sharing of the entrained load between the half-cycles.

2.1 Input water particle kinematics

The formula is designed to predict the net sand transport for given sand characteristics and given current and wave-generated oscillatory flow at the top of the wave boundary layer ($z = \delta$). In general, the bed-parallel velocity due to combined wave and current motion is:

$$\vec{u}(t) = \vec{u}_w(t) + \vec{u}_\delta \tag{3}$$

where $\vec{u}_w(t)$ is the time-varying free-stream orbital velocity vector and $\vec{u}_\delta$ is the steady current velocity vector. For a wave propagating in the x-direction and an obliquely-incident current making an angle φ with the wave direction (Figure 2), the velocity in the x- and y-directions are:

$$u_x(t) = u_w(t) + |u_\delta| \cos\varphi \tag{4}$$

$$u_y = |u_\delta| \sin\varphi \tag{5}$$

respectively. With reference to Figure 1, the velocity vectors at moments of maximum positive and maximum negative orbital velocity are:

$$\vec{u}_c = \left\{u_{cx}\ ,\ u_{cy}\right\} = \left\{\hat{u}_c + |u_\delta| \cos\varphi,\ |u_\delta| \sin\varphi\right\} \tag{6}$$

$$\vec{u}_{\mathrm{t}} = \left\{u_{\mathrm{tx}}\ ,\ u_{\mathrm{ty}}\right\} = \left\{-\hat{u}_{\mathrm{t}} + |u_{\delta}|\cos\varphi,\ |u_{\delta}|\sin\varphi\right\} \tag{7}$$

where $\hat{u}_{\mathrm{c}}$ and $\hat{u}_{\mathrm{t}}$ are the peak crest and peak trough orbital velocities as indicated in Figure 2. We define the representative orbital velocity amplitude $\hat{u}$ and the representative orbital excursion amplitude $\hat{a}$ for the whole flow cycle as follows:

$$\hat{u} = \sqrt{\frac{2}{T}\int_0^T u_{\mathrm{w}}^2(t)\mathrm{d}t} \tag{8}$$

$$\hat{a} = \frac{\hat{u}T}{2\pi} \tag{9}$$

The representative half-cycle orbital velocity for the wave crest, $\tilde{u}_{\mathrm{c,r}}$, and for the wave trough, $\tilde{u}_{\mathrm{t,r}}$, is then:

$$\tilde{u}_{\mathrm{c,r}} = \tfrac{1}{2}\sqrt{2}\hat{u}_{\mathrm{c}} \tag{10}$$

$$\tilde{u}_{\mathrm{t,r}} = \tfrac{1}{2}\sqrt{2}\hat{u}_{\mathrm{t}} \tag{11}$$

(Note that $\tilde{u}_{\mathrm{c,r}}$ equates to the root mean square velocity of a sinusoidal flow with amplitude $\hat{u}_{\mathrm{c}}$; $\tilde{u}_{\mathrm{t,r}}$ equates to the root-mean square orbital velocity for a sinusoidal flow with amplitude $\hat{u}_{t}$.) The representative combined wave-current velocity vectors for each half-cycle are then:

$$\vec{u}_{\mathrm{c,r}} = \left\{u_{\mathrm{c,rx}}\ ,\ u_{\mathrm{c,ry}}\right\} = \left\{\tilde{u}_{\mathrm{c,r}} + |u_{\delta}|\cos\varphi,\ |u_{\delta}|\sin\varphi\right\} \tag{12}$$

$$\vec{u}_{\mathrm{t,r}} = \left\{u_{\mathrm{t,rx}}\ ,\ u_{\mathrm{t,ry}}\right\} = \left\{-\tilde{u}_{\mathrm{t,r}} + |u_{\delta}|\cos\varphi,\ |u_{\delta}|\sin\varphi\right\} \tag{13}$$

The degree of velocity skewness is expressed through the velocity skewness parameter $R = \hat{u}_{\mathrm{c}}/(\hat{u}_{\mathrm{c}} + \hat{u}_{\mathrm{t}})$; similarly, the degree of acceleration skewness is expressed through $\beta = \hat{u}_{\mathrm{c}}/(\hat{u}_{\mathrm{c}} + \hat{u}_{\mathrm{t}})$, where $\hat{u}_{\mathrm{c}}$ and $\hat{u}_{\mathrm{t}}$ are the amplitudes of the horizontal flow acceleration in the crest and trough directions respectively. Orbital velocity for a sinusoidal flow is vertically and horizontally symmetrical, with R = 0.5 and β = 0.5. A typical shoaling wave close to the breaker point (like that schematised in Figure 1), has higher onshore orbital velocity under the wave

crest than offshore velocity under the wave trough, leading to $R > 0.5$, and a forward-leaning wave crest with higher acceleration under the crest compared to the trough, resulting in $\beta > 0.5$.

In the case of irregular wave conditions we adopt the representative wave approach, in which the input water particle kinematics are those for a regular wave with time-series based on $\hat{u} = \hat{u}_{\text{sig}}$, $T = T_{\text{p}}$, $R = R_{\text{sig}}$ and $\beta = \beta_{\text{sig}}$, where $\hat{u}_{\text{sig}}$ is the significant orbital velocity amplitude, T_{p} is peak spectral period, R_{sig} and β_{sig} are the significant values of velocity and accelerations skewness parameter respectively.

2.2 Bed shear stress

The non-dimensional bed shear stress (Shields parameter) vector is:

$$\vec{\theta}_i = \left\{ \theta_{i\text{x}} \ , \ \theta_{i\text{y}} \right\} \tag{14}$$

where subscript "*i*" is either "c" for crest or "t" for trough. The *x* and *y* components of the Shields parameter are:

$$\theta_{i\text{x}} = \left|\theta_i\right| \frac{u_{i,\text{rx}}}{\left|u_{i,\text{r}}\right|} + \frac{\tau_{w\text{Re}}}{(s-1)gd_{50}} \tag{15}$$

$$\theta_{i\text{y}} = \left|\theta_i\right| \frac{u_{i,\text{ry}}}{\left|u_{i,\text{r}}\right|} \tag{16}$$

$\tau_{w\text{Re}}$ is a stress contribution associated with progressive surface waves, which is not present in the case of tunnel-type oscillatory flows, and is explained further below. The magnitude of the Shields parameter is given by:

$$\left|\theta_i\right| = \frac{\frac{1}{2} f_{\text{w}\delta i} \left|u_{i,\text{r}}\right|^2}{(s-1)gd_{50}} \tag{17}$$

in which $f_{\text{w}\delta}$ is the wave-current friction factor. While the transport formula applies to oscillatory flow and current under any angle following the notations, throughout the remainder of this paper the oscillatory flow and current conditions are always collinear, and the presented transport rates based on Eq. (1) are always the *x*-direction transport rates.

Following Ribberink (1998), the wave-current friction factor at crest and trough are calculated as the linear combination of the wave friction factor (at crest and trough) and the current friction factor (see also Madsen and Grant, 1976):

$$f_{w\delta i} = \alpha f_{\delta} + (1-\alpha) f_{wi} \tag{18}$$

with:

$$\alpha = \frac{|u_{\delta}|}{|u_{\delta}| + \hat{u}} \tag{19}$$

The current-related friction factor is calculated assuming a logarithmic velocity profile:

$$f_{\delta} = 2\left[\frac{0.4}{\ln(30\delta/k_{s\delta})}\right]^2 \tag{20}$$

where the current-related roughness $k_{s\delta}$ is calculated as detailed in Appendix A.

The wave friction factor, calculated separately for the crest and trough half-cycles, is based on Swart (1974), modified to allow for enhanced/reduced bed shear stress in acceleration-skewed flow following the approach of Silva et al. (2006):

$$\begin{aligned} f_{wi} &= 0.00251\exp\left[5.21\left(\frac{\left(\frac{2T_{iu}}{T_i}\right)^{c_1}\hat{a}}{k_{sw}}\right)^{-0.19}\right] && \text{for} \quad \frac{\hat{a}}{k_{sw}} > 1.587 \\ f_{wi} &= 0.3 && \text{for} \quad \frac{\hat{a}}{k_{sw}} \le 1.587 \end{aligned} \tag{21}$$

where k_{sw} is the wave-related bed roughness and is detailed in Appendix A. Higher flow acceleration leads to higher peak bed shear stress; as shown in fixed bed (Suntoyo et al., 2008; Van der A et al., 2011) and mobile bed experiments (Ruessink et al., 2011). The term $\frac{2T_{iu}}{T_i}$ in Eq. (21) accounts for the effect of acceleration skewness on the bed shear stress. It has the effect of increasing f_{wi} for the flow half-cycle with higher acceleration ($\frac{2T_{iu}}{T_i} < 1$) and decreasing f_{wi}

for the half-cycle with lower acceleration ($\frac{2T_{iu}}{T_i} > 1$); the term is equal to unity for sinusoidal or pure velocity-skewed flow and Eq. (21) then reduces to the standard Swart equation. Optimisation of c_1 against the measurements of bed shear stress by Van der A et al. (2011) for a range of acceleration-skewed oscillatory flows resulted in c_1 = 2.6. Figure 3 shows the calculated values of the ratio of maximum crest bed shear stress to maximum through bed shear stress using c_1 = 2.6 and the corresponding measured values of the same ratio from the Van der A et al. experiments.

For progressive surface waves, the vertical orbital water particle motions transfer horizontal momentum in and out of the wave boundary layer, leading to a wave-averaged (Reynolds) stress $-\rho\langle\tilde{u}\tilde{w}\rangle$ (Longuet-Higgins, 1953, 1958). The vertical gradient of this stress drives a positive mean flow (boundary layer streaming) in the direction of the wave propagation. Following Nielsen (2006), we account for the wave Reynolds stress, as present at the edge of the wave boundary layer, by adding a wave Reynolds stress $\tau_{w\mathrm{Re}}$ to the *x*-component bed shear stress, as per Eq. (15). This has the effect of increasing the total Shields stress under the wave crest and decreasing the stress under the wave trough. The wave Reynolds stress is estimated as follows (Fredsøe and Deigaard, 1992; Nielsen, 2006):

$$\tau_{\mathrm{w\,Re}} = \rho \frac{f_{\mathrm{w}\delta}}{2c_{\mathrm{w}}} \alpha_{\mathrm{w}} \hat{u}^3 \tag{22}$$

with $\hat{u}$ determined according to Eq. (8), α_{w} = 4/(3π) = 0.424 and c_{w} is the wave speed, calculated from $c_{\mathrm{w}} = L/T$, with L obtained from Soulsby's (1997, p.71) explicit approximation of the dispersion relation. Here $f_{\mathrm{w}\delta}$ is the full-cycle wave-current friction factor, $f_{\mathrm{w}\delta} = \alpha f_\delta + (1-\alpha) f_{\mathrm{w}}$, with f_δ calculated as before and f_{w} is Swart's friction factor calculated as per Appendix A.

2.3 Distributing sediment load between half cycles: phase lag parameter

The sand load entrained during each half-cycle, Ω_i, is calculated using Eq. (2). How much of that sand is transported within the half-cycle and how much remains in suspension to be transported in the following half-cycle is determined by the value of the phase lag parameter for the half-cycle, P_i, as follows:

$$\Omega_{cc} = \begin{cases} \Omega_c & \text{if} \quad P_c \le 1 \\ \dfrac{1}{P_c}\Omega_c & \text{if} \quad P_c > 1 \end{cases} \tag{23}$$

$$\Omega_{ct} = \begin{cases} 0 & \text{if} \quad P_c \le 1 \\ \left(1 - \dfrac{1}{P_c}\right)\Omega_c & \text{if} \quad P_c > 1 \end{cases} \tag{24}$$

$$\Omega_{tt} = \begin{cases} \Omega_t & \text{if} \quad P_t \le 1 \\ \dfrac{1}{P_t}\Omega_t & \text{if} \quad P_t > 1 \end{cases} \tag{25}$$

$$\Omega_{tc} = \begin{cases} 0 & \text{if} \quad P_t \le 1 \\ \left(1 - \dfrac{1}{P_t}\right)\Omega_t & \text{if} \quad P_t > 1 \end{cases} \tag{26}$$

Thus, when the phase lag parameter P_i exceeds 1, there is an exchange of sand from the present half-cycle to the following half-cycle. The phase lag parameter is given by:

$$P_c = \begin{cases} \alpha\left(1 - \dfrac{\xi\hat{u}_c}{c_w}\right)\dfrac{\eta}{2\left(T_c - T_{cu}\right)w_{sc}} & \text{if} \quad \eta > 0 \text{ (ripple regime)} \\ \alpha\left(1 - \dfrac{\xi\hat{u}_c}{c_w}\right)\dfrac{\delta_{sc}}{2\left(T_c - T_{cu}\right)w_{sc}} & \text{if} \quad \eta = 0 \text{ (sheet flow regime)} \end{cases} \tag{27}$$

$$P_t = \begin{cases} \alpha\left(1 + \dfrac{\xi\hat{u}_t}{c_w}\right)\dfrac{\eta}{2\left(T_t - T_{tu}\right)w_{st}} & \text{if} \quad \eta > 0 \text{ (ripple regime)} \\ \alpha\left(1 + \dfrac{\xi\hat{u}_t}{c_w}\right)\dfrac{\delta_{st}}{2\left(T_t - T_{tu}\right)w_{st}} & \text{if} \quad \eta = 0 \text{ (sheet flow regime)} \end{cases} \tag{28}$$

where α is a calibration coefficient, η is ripple height (Appendix B), δ_{si} is sheet flow layer thickness for the half cycle (Appendix C) and w_{si} is the sediment settling velocity within the

half cycle. The term $\frac{r_i}{2\left(T_i - T_{iu}\right)w_{si}}$ represents the ratio of a representative sediment stirring height (r_i = ripple height η or sheet flow layer thickness δ_{si}) and the sediment settling distance within the half cycle. In the ripple regime, the generation and ejection of sediment laden vortices on the ripple sides result in unsteady phase lag effects. The relative importance of the vortex shedding process depends on the size of the vortices and their entrainment height, which scale with the ripple height η (Van der Werf et al., 2006). In the sheet flow regime, where phase lag effects occur predominantly for fine sands, the characteristic entrainment height of the sand scales with the thickness of the sheet flow layer δ_{si}. The above approach for ripple conditions is different from previous half-cycle formulae of Dibajnia and Watanabe (1996) and Silva et al. (2006) in which the effect of ripples on the phase lag parameter is accounted for through a modification of the critical value of P_i for rippled beds.

The sediment settling time is related to the deceleration time within each half cycle, $2\left(T_i - T_{iu}\right)$, thus recognising that with increasing (forward leaning) acceleration skewness the settling time during the crest half-cycle increases, leading to a smaller P_c; analogously the settling time during the trough half-cycle decreases, leading to a larger P_t. This effect was seen in the fine sand sheet flow experiments of Van der A et al. (2009) and in the 1DV model simulations of Ruessink et al. (2009), both for acceleration-skewed flows, but the process is also expected to play a significant role for rippled bed conditions. In the absence of acceleration skewnesss $T_{iu} = T_i/2$ and the settling time reduces to the half-cycle period since $2(T_i - T_{iu}) = T_i$.

Calculation of the sediment settling velocity is based on Soulsby (1997), assuming a suspended sediment size $d_s = 0.8d_{50}$ (Van Rijn, 2007c). However, for the case of progressive surface waves (not tunnel-type oscillatory flow) we include an allowance for possible vertical advection of sediment due to vertical orbital water particle velocities (Kranenburg et al., in press). Although wave-induced vertical velocities are small near the bed, they can be of the same order of

magnitude as the (still-water) sediment settling velocity, especially for fine sand and high waves. In the deceleration phase of the crest half cycle, wave-induced vertical water particle velocities are increasing and are directed downwards, aiding the sediment settling process; in contrast, the settling of sediment during the trough half cycle is reduced due to increasing, upwards-directed wave-induced water particle velocities. Sand settling velocities during the crest and trough half cycles are accordingly adjusted as follows:

$$w_{sc} = w_s - w_{min}(r_c) \tag{29}$$

$$w_{st} = \max(w_s - w_{max}(r_t), 0) \tag{30}$$

where w_s is the (still-water) settling velocity as determined using Soulsby (1997), $w_{min}(r_c)$ is the peak negative vertical water particle velocity at elevation r_c and $w_{max}(r_t)$ is the peak positive vertical water particle velocity at elevation r_t. $\hat{w}_c$ and $\hat{w}_t$ are estimated using Stokes 2nd order wave theory and the selected elevation is $r_i = \eta$ in the ripple regime and $r_i = \delta_{si}$ in the sheet-flow regime. For tunnel-type oscillatory flow $w_{sc} = w_{st} = w_s$.

The terms $\left(1 - \frac{\xi \hat{u}_c}{c_w}\right)$ and $\left(1 + \frac{\xi \hat{u}_t}{c_w}\right)$ in Eq. (27) and (28) (where c_w = wave speed, ξ = calibration factor) account for a second effect of progressive waves on the phase lag behaviour: that of horizontal sediment advection caused by horizontal non-uniformity in the wave field. The wave non-uniformity produces horizontal gradients in the horizontal sediment flux, with the result that sediment concentration is no longer controlled by local vertical sediment fluxes alone (i.e. pick-up from and deposition to the bed). Kranenburg et al. (in press) show how this intra-wave horizontal sediment advection leads to a "compression" of sand (increased concentration) under the wave crest and a "dilution" (decreased concentration) under the wave trough, causing a net transport rate in the direction of wave propagation, even for sinusoidal waves. The importance of this transport mechanism for progressive surface waves is shown with a numerical boundary layer model (based on advection-diffusion for the sediment) applied to the

large wave flume experimental conditions of Schretlen et al. (2011). Kranenburg et al. (in press) show that the effect of horizontal sediment advection can be accounted for via correction of the phase-lag parameter through the adjustment time scale T_A:

$$T_A = \frac{\Delta}{w_s}\left(1 - \frac{\xi u_w(t)}{c_w}\right) \tag{31}$$

where Δ/w_s is the ratio of sediment stirring height and settling velocity, representing the settling time of sediment; $u_w(t)$ is the free-stream horizontal flow velocity in the transport layer near the bed; and ξ is a coefficient accounting for the shape of the velocity and concentration profile. A short description of the analytical background of this time scale is presented in Appendix D (see Kranenburg et al., in press for more details). The factor $\left(1 - \frac{\xi u_w(t)}{c_w}\right)$ represents the influence of horizontal sediment advection. It is < 1 under the wave crest and >1 under the wave trough and therefore represents a decrease of the adjustment time scale under the wave crest (i.e. a quicker reaction of the concentration to changes in the velocity) and an increase of adjustment time scale under the wave trough. The factor is significant only when waves are large with relatively high orbital flow velocities $u_w(t)$ compared to the wave speed c_w. Moreover, it can only become effective if phase-lag effects are important, or in other words, the adjustment timescale T_A should not be negligible compared to the wave period T. Based on this result, the effect of horizontal sediment advection is incorporated in the sand transport formula through a correction of the phase-lag parameters P_i for the wave crest and trough, using a factor $\left(1 - \frac{\xi \hat{u}_c}{c_w}\right)$ for the settling time of the crest load and a factor $\left(1 + \frac{\xi \hat{u}_t}{c_w}\right)$ for the settling time of the trough load as per Eqs. (27) and (28). We use coefficient ξ as calibration parameter in this simplified parameterisation (see below).

2.4 Graded sands

For graded sand conditions a fractional approach is used to calculate the net sand transport as follows:

$$\vec{\Phi} = \frac{\vec{q}_s}{\sqrt{(s-1)gd_{50}^3}} = \sum_{j=1}^{M} p_j \frac{\vec{q}_{s,j}}{\sqrt{(s-1)gd_j^3}} \tag{32}$$

where $q_{s,j}$ is the net transport rate of fraction j with diameter d_j, and percentage p_j of that fraction in the bed material, and M is the number of size fractions in the bed material.

Van Rijn (2007c) discussed whether the roughness of each fraction should be based on the grain diameter of the fraction ($k_{s,j} \sim d_j$), or whether for each fraction the same roughness (and hence bed shear stress τ) based on the median grain diameter of the mixture ($k_s \sim d_{50}$) should apply. The first approach assumes segregation of the fractions during the experiment, while in the second approach the bed is assumed to remain well-mixed. Using a multi-fraction approach (including hiding/exposure effects discussed below), Van Rijn (2007c) compared predicted net transport rates from his quasi-steady formulae using both approaches with the medium sand results of Hassan (2003). Best results were obtained with $k_{s,j} \sim d_j$, in agreement with the observed segregation processes during the majority of Hassan's (2003) graded sand experiments. In the present formula, assuming $k_{s,j} \sim d_j$ in the transport rate calculations for each fraction also lead to best agreement with the measured net transport rates. In calculating the fractional transport rate, the phase lag parameter also depends on the grain size of the fraction, therefore:

$$P_{c,j} = \begin{cases} \alpha\left(1 - \dfrac{\xi \hat{u}_c}{c_w}\right) \dfrac{\eta}{2(T_c - T_{cu}) w_{sc,j}} & \text{if } \eta > 0 \text{ (ripple regime)} \\ \alpha\left(1 - \dfrac{\xi \hat{u}_c}{c_w}\right) \dfrac{\delta_{sc}}{2(T_c - T_{cu}) w_{sc,j}} & \text{if } \eta = 0 \text{ (sheet flow regime)} \end{cases} \tag{33}$$

$$P_{t,j} = \begin{cases} \alpha\left(1 + \dfrac{\xi \hat{u}_t}{c_w}\right) \dfrac{\eta}{2(T_t - T_{tu}) w_{st,j}} & \text{if } \eta > 0 \text{ (ripple regime)} \\ \alpha\left(1 + \dfrac{\xi \hat{u}_t}{c_w}\right) \dfrac{\delta_{st}}{2(T_t - T_{tu}) w_{st,j}} & \text{if } \eta = 0 \text{ (sheet flow regime)} \end{cases} \tag{34}$$

In which the settling velocity is based on the particle settling velocity for each fraction individually. The representative entrainment height (either η or δ_{si}) is the same for each fraction and is based on the overall d_{50}.

It is well known that for beds consisting of different size fractions, the finer particles tend to "hide" between the larger particles and therefore have reduced mobility compared to a uniform sand of the same diameter. At the same time coarser particles become more exposed to the flow and are more easily mobilized. These grain sorting effects can be accounted for by applying a correction factor, often as a function of d_j/d_{50}, to the critical Shields parameter and/or the effective Shields parameter (see e.g Hassan, 2003; Van Rijn, 2007c). Correcting the critical Shields parameter only has significant influence on conditions near the threshold of motion. For relatively large Shields parameters, such as for the present sheet flow conditions, an adjustment to the Shields parameter has a greater impact. We apply the correction $\varepsilon_{\text{eff},j}$ to calculate the effective Shields parameter for the fraction with grain size d_j as follows:

$$\left|\theta_{i,j,eff}\right| = \varepsilon_{eff,j}\left|\theta_{i,j}\right| \tag{35}$$

where, as before, $i = c$ (crest) or t (trough), and $\left|\theta_{i,j}\right|$ is the Shields parameter for fraction j, which feeds into the calculation of the sediment load as follows:

$$\Omega_{i,j} = \begin{cases} 0 & \text{if } \left|\theta_{i,j,eff}\right| \le \theta_{\text{cr},j} \\ m\left(\left|\theta_{i,j,eff}\right| - \theta_{\text{cr},j}\right)^n & \text{if } \left|\theta_{i,j,eff}\right| > \theta_{\text{cr},j} \end{cases} \tag{36}$$

with $\theta_{\text{cr},j}$ the critical Shields parameter, according to Soulsby (1997), for fraction j. Following Van Rijn (2007c), the correction factor is defined as:

$$\varepsilon_{eff,j} = \left(\frac{d_j}{d_{50}}\right)^{0.25} \tag{37}$$

This simple correction factor is adapted here in preference to the more commonly used correction factor of Day (1980) which requires information on the gradation of the sand mixture.

2.5 Calibration

The limited applicability of many existing practical formulae is, to some extent, the result of the limited range of flow and sand conditions used to develop the formulae. For this reason Van der

Werf et al. (2009) brought together a large dataset of existing net transport rate measurements from a number of facilities covering a wide range of sand sizes and full-scale flow conditions (the "SANTOSS database"). The database has recently been extended to include more recent net transport measurements for acceleration-skewed oscillatory flows (Van der A et al., 2010; Silva et al., 2011) and for progressive surface waves (Schretlen et al., 2011). The entire dataset contains 226 measured net transport rates for a wide range of full-scale ($T \geq 4$s) conditions in both the rippled bed and sheet flow regime, including regular and irregular oscillatory flows with velocity skewness or acceleration skewness (or a combination of both), oscillatory flows with superimposed collinear currents and non-breaking (shoaling) surface waves. Table 1 presents an overview of the range of hydraulic conditions covered by the data. In most of the oscillatory flow + current experiments (43 out of 50 cases), the current was weak relative to the orbital velocity, $|u_\delta|/\hat{u} < 0.5$, so that in general the experimental conditions for which measured net transport rates are available are oscillatory flow-dominated, not current-dominated. The extended database was used for the calibration of the present practical sand transport formula.

The calibration procedure is an iterative procedure involving three main calibration coefficients: (i) the coefficient α in the phase lag parameter (Eqs. (27) and (28)) for sheet flow and rippled bed conditions; (ii) the proportionality constant m in the sediment load formula (Eq. (2)), and (iii) the power of the excess Shields parameter n in the sediment load formula. In the calibration procedure, α was tuned to find the highest correlation between the measured and predicted transport rates; m was then found from least square fitting a straight line with zero intercept to the measured and predicted net transport rates values, repeating for different values of coefficient n. Once an initial calibration was completed, several subsets of the data were examined and calibration coefficients specific to each subset (p, μ and ζ) were tuned individually to obtain best agreement between measured and predicted transport rates for each particular subset of data. After this m, n and α were adjusted again to obtain best overall

agreement. The entire procedure was repeated several times, finally resulting in: α = 8.2, m = 11.0 and n = 1.2.

3.0 CALCULATED AND MEASURED NET TRANSPORT RATES

In this section we compare calculated net transport rates with measured transport rates for particular sub-datasets (see Table 1) in order to highlight i) the different transport mechanisms that are captured in the formula, and ii) the performance of the formula for each sub-dataset.

3.1 Velocity-skewed oscillatory sheet flow with $d_{50} \geq 0.20$mm

Figure 4 shows a comparison of the measured and calculated transport rates for the 32 pure velocity-skewed sheet flow conditions with $d_{50} \geq 0.20$mm contained in the SANTOSS database. Nearly all transport rates for velocity-skewed conditions are calculated within a factor 2 of the measurements. In addition to the percentage of the data falling within a factor 2, Table 2 lists the factor 5 percentage, the Brier skill score, the bias and the squared correlation coefficient r^2 (see caption). All performance criteria indicate the excellent agreement between the measurements and prediction for these conditions. With the exception of one of Ribberink and Al-Salem's (1994) conditions (indicated by the arrow in Figure 4), for all these experiments with medium and coarse sand ($d_{50} \geq 0.20$mm) $P_i \leq 1$, which means unsteady phase lag effects do no play a role in the predicted transport.

3.2 Acceleration-skewed oscillatory sheet flow with $d_{50} \geq 0.20$mm

Figure 5 shows a comparison between calculated and measured net transport rates for the 32 pure acceleration-skewed oscillatory flow conditions with $d_{50} \geq 0.20$mm. The calculated transport rates show good agreement with the measurements, with 84% of the predictions fall within a factor 2 of the measurements (also see Table 2 for further details). The formula incorrectly calculates the transport direction for one of Watanabe and Sato's (2004) conditions. Due to its forward-leaning acceleration skewness (β = 0.6), a positive net transport rate is

calculated, in contrast to their measured negative net transport rate. The discrepancy may be due to measurement error: Watanabe and Sato (2004) determine their net transport rate on the difference between the masses of sand collected at the ends of the test section, a method that is more prone to measurement error than the method based on mass conservation applied to the whole test section as used in most other studies. For some of Watanabe and Sato's (2004) conditions (indicated with the grey symbols), the relatively short flow period of T = 5s combined with large orbital velocities ($u_{w,max}$ ~ 1.45m/s) results in phase lag effects contributing significantly to the net transport rates (i.e. $P_i > 1$). Watanabe and Sato's own observations of the time-dependent sand concentrations confirm the occurrence of the unsteady behaviour. No phase lag effects were observed for the same sand size and orbital velocities for flow periods of 7 and 10s, which provide longer settling times (Silva et al., 2011). The transport formula is able to capture these processes.

3.3 Oscillatory sheet flow for fine sands (d_{50} < 0.20mm)

Figure 6 shows the calculated net transport rates for the 29 oscillatory sheet flow conditions with d_{50} < 0.20mm. The conditions include the pure acceleration-skewed flows of Van der A et al. (2010), for which the measured net transport rates are all onshore-directed, while the remaining conditions are all pure velocity-skewed flows for which the measured net transport rates are predominantly negative, or "offshore"-directed. For both flow types, the experimental studies have shown that unsteady phase lag effects dominate the transport rate direction, which is calculated correctly by the formula for nearly all conditions. Although the magnitudes of the net transport rates are somewhat underpredicted, they agree reasonably well with measurements: 86% of the calculated transport rates are falling within a factor 2 of the measurements, with the exception of several of the velocity-skewed oscillatory flows. The scores for the various performance criteria listed in Table 2, reinforce these conclusions. Note that not invoking the sheet-flow enhancement to the fine sand roughness (i.e. setting μ = 1 in Eq. (A.1)) results in significant under-estimation of the net transport rate, with only 38% of the calculated transport rates falling within a factor 2 of the measurements.

3.4 Oscillatory flow over rippled beds

When the bed is rippled, the bed roughness $k_{sw,r}$ can be expected to scale with the ripple dimensions. Common practice is to scale the roughness to the ripple height $k_{sw,r} \sim \eta$ (Van Rijn, 2007a; Humbyrd and Madsen, 2010) or to the product of ripple height and ripple steepness as follows:

$$k_{sw,r} = p\eta\frac{\eta}{\lambda} \tag{38}$$

where λ is ripple length and p a constant. Values of p reported in the literature cover a wide range between 8 – 28 (e.g. Nielsen, 1983; Raudkivi, 1988; Swart, 1976; Grant and Madsen, 1982). p has no physical meaning and its variability may be attributed to the choice of friction factor formula as suggested by Humbyrd and Madsen (2010). For the present formula p is used as a specific calibration factor for the net transport rate prediction over rippled beds. Based on comparison of the measured and calculated net transport rates for the rippled bed conditions, an optimal value of p = 0.4 was found (see Eq. (A.5)). Note that in calibrating p the measured ripple dimensions from the experiment have been used to avoid errors inherent in using an empirical ripple predictor.

Figure 7 shows the comparison of the measured and calculated net transport rates, using measured ripple dimensions as input, with corresponding performance criteria listed in Table 2. Despite the scatter in these results, the net transport rates are considered to be reasonably well calculated. It should be emphasised here that prediction of net transport rates for rippled beds is notoriously difficult, due to the unsteady effects associated with the complex flow structure over ripples, and because the net transport rates are low. Van der Werf et al. (2006) compared predicted net transport rates from the grab-and-dump model of Nielsen (1998), the semi-unsteady formula of Dibajnia and Watanabe (1996) and their own semi-unsteady formula with the same ripple condition experimental data as used for Figure 7 and found that for the best model only 35% of the predictions fell within a factor 2 of the measurements. Similarly, Silva et al. (2006) found only 47% of their predictions to fall within a factor 2, while 20% of their

predictions failed to determine the correct transport direction. In contrast, 62% of the calculated net transport rates from the present formula are within a factor 2 of the measurements and the correct direction is calculated for 91% of the conditions. When the predicted ripple dimensions based on O'Donoghue et al.'s (2006) predictor (see Appendix B) are used as input to the formula, 40% of the calculated transport rates would fall within a factor 2 of the measurements, and the direction is correct for 80% of the conditions. We note that the O'Donoghue et al. (2006) ripple predictor applies to equilibrium ripples under waves and oscillatory flows without current. For non-equilibrium ripples and flows with current the more recent predictor of Soulsby et al. (2012) may be considered; the Soulsby et al. predictor also includes a simple approach to account for bio-degradation effects on the ripple height.

3.5 Oscillatory flow with superimposed current

Figure 8 shows the comparison of measured and calculated net transport rates for conditions of oscillatory flows with current. The calculated transport rates show reasonable agreement with observations: 70% of the 50 conditions fall within a factor 2 of the measurements; more detailed metrics are presented in Table 2. Negative net transport rates are generally calculated for conditions where a net current opposes the (implied) wave direction (conditions of Dibajnia and Watanabe, 1992; Ribberink, 1995; Silva et al., 2011), while most positive calculated and measured net transport rates occur when currents follow the (implied) wave direction. The good correlation (r^2 = 0.89) suggests that the behaviour is well captured, despite a general over-estimation of the net transport rates indicated by the large positive bias for these conditions (*bias* = 61%).

It should be noted that for the non-sinusoidal oscillatory flow with current conditions in the database, the measured mean velocity, could contain a streaming velocity (generated by the asymmetry in turbulence intensity between the two half-cycles), in addition to the superimposed current velocity. This type of streaming is present under oscillatory flow with velocity skewness (e.g. Ribberink and Al-Salem, 1995) and under oscillatory flows with acceleration skewness (Van der A et al., 2011). The transport formula accounts implicitly for this type of streaming,

which could mean that the effect of streaming on the predicted net transport rate is accounted for twice for some of the non-sinusoidal oscillatory flow with current conditions.

3.6 Oscillatory flow and graded sands

Figure 9 shows the measured and calculated net transport rates for graded sediment conditions, for which the details of the sand mixtures can be found in Table 3. Considering the wide range of d_{50} of the mixtures and that the conditions cover oscillatory flows and oscillatory flows plus current, the calculated net transport rates are in good agreement with measurements, with 89% within a factor 2 of the measurements (Table 2). The roughness for the sheet flow conditions in the model for graded sands is calculated without the fine sand adjustment (μ = 1 in Eq. (A.1)), which improves results compared to those based on the roughness including the fine sand enhancement.

3.7 Progressive surface waves

The influence of the following three 'real wave' processes is included in the transport formula (see Section 2.0): 1) vertical advection of horizontal momentum leading to progressive wave boundary layer streaming and a wave-averaged stress; 2) horizontal gradients in horizontal sediment flux leading to horizontal sediment advection, and 3) near-bed vertical orbital velocities and their effect on grain settling.

Figure 10 shows the calculated and measured net transport rates for the 11 surface wave conditions included in the database, consisting of 7 medium sand conditions and 4 fine sand conditions in two available dataset (Dohmen-Janssen and Hanes, 2002; Schretlen et al. 2011). All conditions are in the sheet flow regime and the near-bed flow is dominated by velocity-skewness in all cases. For the medium sand cases, there is reasonable agreement between the calculated and measured transport rates, although distinct differences exist between the two datasets. The differences may be caused by the fact that, although d_{50} was the same for both

datasets (d_{50} = 0.25mm), d_{90} was considerably larger for the Schretlen experiments (0.42mm as against 0.28mm). For the fine sand conditions, the calculated net transport rates are in the positive (onshore) direction, which is in agreement with the wave flume measurements, but which is opposite to the negative (offshore) transport measured for fine sand velocity-skewed flows in oscillatory flow tunnels (see Section 3.2). Only the fine sand cases are affected by phase-lag effects, and best results are obtained with coefficient ξ = 1.7 in Eqs. (33) and (34). Overall, the agreement between the calculated and measured net transport rates for the 11 experiments is good: 82% of the predictions fall within a factor 2 of the measurements.

If the 'real wave' effects are switched off, the calculated net transport rates for the medium sand would be positive, but slightly lower in magnitude due to the absence of the positive wave Reynolds stress (advection processes are negligible for medium sand). For the fine sand conditions on the other hand, the net transport would be negative similar to many of the fine sand velocity-skewed oscillatory flow conditions.

In summary, it is shown that under progressive surface waves generally more sand is transported in the positive (onshore) direction than in flow tunnels, especially for fine sand. By incorporating three different (momentum and sediment) advection processes in the transport formula in a parameterized way, a practical method is obtained to predict the enhanced transport rates.

4.0 NET TRANSPORT BEHAVIOUR WITH u_{rms}

Figure 11 illustrates the behaviour of the calculated non-dimensional net transport rates with u_{rms} ($=\hat{u}/\sqrt{2}$) for two idealised oscillatory flow conditions (a-b) and two progressive surface wave conditions (c-d). The flow period is constant with T = 6.5s and for all four conditions net transport rates are shown for two sand sizes, fine sand with d_{50} = 0.13mm and medium sand with d_{50} = 0.25mm. For ripple regime conditions, the ripple dimensions are predicted using O'Donoghue et al. (2006) (see Section 3.4). For comparison, measured net transport rates from

experimental studies listed in Table 1 are added to Figure 11 where the experimental conditions are close to those used for the calculated transport rates in terms of T, R and β, grouped into fine (d_{50} < 0.20mm) or medium sand (0.20mm ≤ d_{50} < 0.30mm). Because the experimental conditions do not exactly agree with the conditions used for the calculated transport rates, they do not serve for direct quantitative comparison; the purpose in showing the experimental results is simply to demonstrate experimental confirmation of the trends predicted by the formula.

Figure 11a shows the net transport behaviour for velocity-skewed oscillatory flow with R = 0.62. For low u_{rms} the medium sand net transport rates are negative and dominated by phase-lag effects in the rippled bed regime. When u_{rms} increases further, the regime shifts from rippled bed to sheet flow, where the net transport rates become positive and increase with increasing velocity. The fine sand net transport behaviour is negative at low u_{rms} when the bed is rippled. It becomes positive with increasing u_{rms}, before becoming negative again as a result of strong phase lag effects in the sheet flow regime. This behaviour is in agreement with the measurements.

Figure 11b shows the net transport rates for an oscillatory flow with a degree of acceleration skewness (β = 0.7) but without velocity skewness (R = 0.5). For this flow the medium sand net transport rates are positive in the ripple regime, because, in contrast to the velocity-skewed flow, phase lag effects related to the timing of the flow maxima augment the positive transport, although there is presently no experimental data to confirm this behaviour. When entering the sheet flow regime (here at u_{rms} ≈ 0.65m/s) the net transport rates initially reduce, in part due to a decreased roughness caused by decreasing ripples dimensions, and partly because the phase lag effects disappear. Once fully in the sheet flow regime, net transport rates increase in a quasi-steady manner with increasing u_{rms}, which is in agreement with the measurements. Fine sand net transport rates are also positive in the ripple regime, and remain positive in the sheet flow regime, in strong contrast to the negative sheet flow net transport rates seen for velocity-skewed flows.

Figure 11c shows the net transport rate behaviour for a surface wave with velocity skewness R = 0.62, similar to the oscillatory flow in Figure 11a. Comparison of both figures shows that the

surface wave effects nearly always result in positive net transport rates. This is in contrast to the observations and predictions for velocity-skewed oscillatory flows. Net transport rates are only negative in the ripple regime for the fine sand at low flow velocities. For the fine sand at larger velocities, and for the medium sand, the net transport rates are positive in the ripple regime, due to the additional positive (onshore) contributions of the surface wave effects. Discontinuities in the medium sand curve at $u_{rms} \approx 0.5$ m/s indicate the switch from the ripple regime to the sheet flow regime, causing strong changes in the roughness and the phase lag parameter as discussed before. For medium sand in the sheet flow regime ($u_{rms} >\sim 0.6$m/s), transport behaviour is increasing quasi-steadily with u_{rms}, and net transport rates are larger by about 50% compared to the equivalent oscillatory flow, due to the surface wave effects. Fine sands show larger transport rates than medium sands in the sheet flow regime, a trend which is only qualitatively confirmed by the data.

Finally, although experimental evidence of the trends is not available, Figure 11d shows net transport rates for a surface wave with both velocity and acceleration skewness, typical for near-shore waves close to breaking. The added effects of acceleration skewness lead to an added positive contribution to the net transport, both for rippled bed and sheet flow. For fine sands in the ripple regime this added component leads to positive net transport rates for all u_{rms}, while for the remaining conditions it leads to even larger positive net transport rates compared to the purely velocity-skewed condition in Figure 11c. Apart from this, the behaviour with increasing u_{rms} is similar to that shown in Figure 11c.

5.0 VALIDATION

5.1 Oscillatory flow

Development and calibration of the formula has been done against the data contained in the SANTOSS database as described in Section 2.0. The database has since then been extended with conditions previously not considered, namely the conditions from the Tokyo University

oscillatory flow tunnel experiments of Dibajnia and Kioka (2000) and Dibajnia et al. (2001). These conditions have been excluded from the calibration and are instead used here to test the validity of the new formula to a certain degree. To extend the limited number (8) of conditions which satisfy the SANTOSS database criteria of $T \geq 4$s, we have also included conditions falling within the $3.5 < T < 4$s range. By extending this lower limit of acceptable flow periods, the Tokyo University flow tunnel data of Sato (1987) and Dibajnia and Watanabe (1998) also satisfy the selection criteria. Combined, these datasets give 58 different conditions and cover a wide range of irregular oscillatory flows, sand sizes and bed conditions, the details of which are outlined in Table 4. Note that all of these validation cases involve irregular oscillatory flow.

The comparison of measured and calculated net transport rates for these conditions (see Figure 12), shows good agreement. The transport direction of Sato's (1987) fine sand rippled-bed conditions, which have mostly negative net transport rates related to phase lag effects, are nearly all correctly calculated. The positive sheet flow net transport rates are generally calculated within a factor 2 of the measurements, although an overestimation for the conditions with flow periods in the range $3.5\text{s} < T < 4\text{s}$ is apparent. Out of the 58 conditions, 66% are calculated within a factor 2 of the measurements, which is a slight improvement compared to the irregular flow conditions listed in Table 2.

5.2 Steady flow

When the wave height is zero and the transport is driven by current only and $\alpha = 1$ (Eq. (19)), $f_{w\delta i} = f_\delta$ (Eq. (18)) and $u_{i,r} = u_\delta$, consequently:

$$\theta_\delta = \frac{\frac{1}{2} f_\delta u_\delta^2}{(s-1) g d_{50}} \tag{39}$$

and the transport formula Eq. (1) reduces to the following formula, resembling the Meyer-Peter and Müller bedload transport formula (see also Ribberink, 1998):

$$\Phi = \sqrt{\theta_\delta}\,\Omega_\delta = \sqrt{\theta_\delta}\, m\left(\theta_\delta - \theta_{cr}\right)^n \tag{40}$$

Figure 13 illustrates the performance of the formula in predicting the net transport rates for the steady flow data of Guy et al. (1966), Van den Berg (1986) and Nnadi and Wilson (1992). These data have not been used in the calibration of the present formula. For most of the open channel experiments of Guy et al. (1996) the Shields number θ_δ was < 1 and bedforms were present, while for most of the Nnadi and Wilson (1992) duct experiments the Shields number θ_δ was > 1 and the bed was completely flat. Similar to Ribberink (1998), we only use the bed-load transport rates of Guy et al. (1996) that were obtained by subtracting the measured suspended load from the measured total load, and for Nnadi and Wilson, for which the majority of transport took place in the (near-bed) sheet flow layer, we use the reported total transport rates. The field data of Van den Berg (1986) involve low Shields numbers (θ_δ < 0.3), and bed-load transport rates obtained from dune migration measurements. Combined the datasets comprise 137 sheet flow and dune conditions with current velocities ranging 0.32-2.03 m/s and median grain sizes 0.19-3.8mm. The results and quantitative performance measures shown in Figure 13 show that the formula predicts net transport rate for current-only conditions well, with 85% of the 137 conditions calculated within a factor 2 of the measurements.

6.0 DISCUSSION

For oscillatory flow or waves with superimposed current the transport formula requires information about the magnitude and direction of the mean current velocity at a reference level $z = \delta$, i.e. at the top of the wave boundary layer. For the calibration and validation results presented here, a constant value of δ = 0.20m was used, which for all measurements was well above the wave boundary layer. Since the wave boundary layer thickness depends on the relative roughness ($\hat{a}/k_{sw}$), it would have been more realistic to estimate δ for each condition using an appropriate formula for the boundary layer thickness (e.g. Sleath, 1987; Van der A et al. 2011). However, the influence of δ on the net transport rate is rather small, as shown in Figure 14.

The formula covers a wide range of flow conditions and sand sizes that occur in typical sandy coastal environments. It specifically takes into account the influence of varying wave shape (velocity and acceleration skewness) and unsteady phase-lag effects in the wave boundary layer. Nevertheless, application of the formula in practice may still be subject to restrictions, due to a lack of reliable net transport data for specific regimes. This especially holds for (full-scale) surface waves and acceleration-skewed oscillatory flows over rippled beds, for waves with strong superimposed currents and waves with currents under an angle.

In case of waves with or without superimposed currents the transport formula describes the bed load and suspended load transport in the wave boundary layer. For non-breaking waves and relatively small mean currents, such as those conditions in the database, almost all of the sand transport takes place inside the wave boundary layer and so the transport formula describes the total transport rate for these conditions. For stronger superimposed currents and large flow depths (e.g. tidal flow) or estuarine situations where currents are relatively large compared to the waves, sand may go into suspension to levels well above the wave boundary layer, in which case a separate suspended transport model should be added to the transport formula to account for the current-related suspended load above the wave boundary layer. For current only conditions, the formula calculates the transport in the sheet flow layer for sheet-flow conditions and the bed-load transport for non sheet-flow conditions, in accordance with the data used in Section 5.2. If there is significant sediment in suspension above the sheet flow layer or bed-load layer, a separate suspended load model is also needed to calculate the suspended load transport. Assuming a morphodynamic model application, our recommended method is to use a 3D or quasi-3D advection-diffusion model to describe the mean concentration profile, $\langle C(z) \rangle$, above a prescribed reference level, z_{ref}, using a reference concentration and sediment mixing coefficient description, as for example given by Van Rijn (1993, 2007b), Soulsby (1997) or Zyserman and Fredsøe (1994). Using this in conjunction with the mean-current profile, $\langle \vec{u}(z) \rangle$, the suspended load transport can be computed by integration from a lower near-bed level, z_l, to the mean water level z_w:

$$\vec{q}_{s,susp} = \int_{z_l}^{z_w} \langle C(z) \rangle \langle \vec{u}(z) \rangle dz \qquad (41)$$

In wave-current conditions two situations may occur:

(i) $z_{ref} < \delta$: This will generally occur in wave-dominated conditions in the ripple or sheet flow regime. For example, Van Rijn (1993) selects the reference level at the upper edge of the sheet flow layer or at ripple-crest level, which is always inside the wave boundary layer. In this situation it is recommended to use $z_l = \delta$ in the integration.

(ii) $z_{ref} > \delta$: This situation may occur when large bedforms, e.g. current-induced dunes, are treated as bed roughness (not resolved by the computational grid) and the reference level is selected at the level of the dune crests (Van Rijn, 1993). In this situation it is suggested to use $z_l = z_{ref}$ as a practical solution.

The formula is restricted to non-breaking wave conditions. Net sand transport rates for breaking wave conditions are often calculated using a transport formula for horizontal oscillatory flow, sometimes extended with additional sediment stirring to account for breaking-induced turbulent kinetic energy near the bed (Roelvink and Stive, 1989; Butt et al., 2004). Inclusion of a stirring effect is supported by experimental studies showing increased turbulent mixing and increased suspended sediment load due to wave breaking (Deigaard et al., 1986; Van Rijn, 2007b). However, the transport processes under breaking waves are expected to be further complicated by flow non-uniformity and suspended sediment advection, leading to suspended sediment transport that is not wholly determined by the local flow conditions (Kobayashi and Jonsson, 2001). Despite these insights, existing sand transport formulae for breaking waves are still speculative due to the lack of measurements of net sand transport rates and of the detailed sand transport processes, in particular under full-scale waves.

The least good agreement with the measurements, in terms of percentage of the predictions falling within a factor 2 of the measurements, is found for irregular flows (Table 2). Most of these conditions involved velocity-skewed irregular oscillatory flows over rippled beds and calculated net transport was based on the "representative wave", using the significant velocity

characteristics and peak flow period, as described in Section 2.1. The skill score for these conditions is rated fair (*BSS* = 0.54), and only 57% of the conditions fall within a factor 2 of the measurements. These rather low scores may be due to effects of flow irregularity that are not captured in our representation of the irregular flow time-series by one regular flow cycle. It is likely that time-history effects, for example caused by the "pumping up" of suspended sediment in irregular wave sequences (Vincent and Hanes, 2002), make a representative wave approach unsuitable, especially in situations with strong phase lag influence. Whether a wave-by-wave approach leads to better net transport rate predictions compared to the representative wave approach in such situations, or in fact whether a representative wave approach should be based on other than significant wave characteristics that we adopted here could not be determined from the available dataset, and remains subject of future research.

The net transport in the wave boundary layer is affected by the slope of the bed through gravity effects. This may change the effective critical bed shear stress as well as the magnitude and direction of the boundary layer flow and effective bed shear stress, and therefore also the magnitude and direction of the net transport. The data used for the development of the present formula is limited to horizontal bed conditions only, i.e. the effect of bed slope is presently not included the formula. Apsley and Stansby (2008) propose a generalized model for slopes smaller than the angle of repose with arbitrary orientation with respect to the wave and current direction. Although the method is not validated for oscillatory flows yet, it is suggested to use this method in the present formula.

Due to an absence of reliable net transport data from the field a direct comparison of the formula against field conditions is not yet feasible. An indirect test against field conditions can be carried out by implementation of the formula within a morphodynamic model, which ultimately is its intended application. While ongoing work is aimed at implementing the formula in a 3D morphodynamic model in order to compare it with field data, as a first step in this process the formula has been implemented in a cross-shore morphodynamic model applied to wave flume cases, which showed encouraging results (Van der Werf et al., 2012). This exercise did however reveal that good transport rate predictions rely on accurate predictions of the orbital

velocity characteristics, especially regarding the velocity and acceleration skewness. In morphodynamic models the sand transport formula should therefore be used in conjunction with velocity parameterizations that include both velocity and acceleration skewness, and which can be linked to local wave and beach parameters (e.g. Ruessink et al., 2012; Malarkey and Davies, 2012).

7.0 CONCLUSION

A new practical formula for net sand transport induced by non-breaking waves and non-breaking waves with collinear currents has been presented. The formula is based on Dibajnia and Watanabe's (1992) semi-unsteady half-cycle concept, which accounts for the transport contribution related to unsteady phase lag effects within the wave boundary layer, and has bed shear stress as the main forcing parameter. The formula distinguishes itself from other semi-unsteady half-cycle-type formulae through explicit inclusion of surface wave effects, details in the process calculations and the extent of the experimental data used to develop the formula.

The formula is developed using a database of 226 net transport rate measurements from large-scale oscillatory flow tunnels and a large wave flume, covering a wide range of full-scale flow conditions and uniform and graded sands with median diameter ranging from 0.13mm to 0.54mm. Good overall agreement is obtained between observed and predicted net transport rates with 78% of the predictions falling within a factor 2 of the measurements. The formula has been validated against independent net transport rate data for oscillatory flow conditions and bedload-dominated steady flow conditions.

The formula performs best for regular oscillatory sheet flow conditions, with and without currents, involving uniform fine, coarse and graded sands. Formula performance for other conditions - rippled beds, irregular flows, progressive surface waves - is reasonable but less good. The difference in performance for different conditions can be partly attributed to the unequal number of the various conditions within the database of experimental results (Table 1). But poorer performance is also likely to be partly due to insufficient understanding of the

detailed sand transport processes, and this remains particularly true for progressive surface wave conditions, for which reliable detailed data is difficult to obtain.

Arguably, the most significant shortcoming in the new formula is that it is based entirely on oscillatory flows and non-breaking surface waves. Accordingly, although the model as constructed could in principle be applied to breaking waves as long as the hydrodynamics at the top of the wave boundary layer can be provided as input, net transport rates for breaking wave conditions cannot be calculated with any degree of confidence. A main goal of future research therefore is to extend the range of large-scale laboratory experiments to include breaking wave conditions and, based on the experimental results, to adapt the formula to account for the breaking wave processes.

The SANTOSS database of measured net transport rates for large-scale oscillatory flow and surface wave conditions and a MATLAB code for implementation of the new, so-called SANTOSS formula are available on request to the authors.

ACKNOWLEDGEMENTS

This work is part of the SANTOSS project ('SANd Transport in OScillatory flows in the Sheet-flow regime') funded by the UK's EPSRC (GR/T28089/01) and STW in The Netherlands (TCB.6586). JW acknowledges Deltares strategic research funding under project number 1202359.09. Richard Soulsby is gratefully acknowledged for valuable discussions and feedback on the formula during the SANTOSS project.

APPENDIX A: *Current-related and wave-related bed roughness*

Following Ribberink (1998) the current-related bed roughness is given by:

$$k_{s\delta} = \max\{3d_{90}, d_{50}[\mu + 6(\langle|\theta|\rangle - 1)]\} + 0.4\eta^2 / \lambda \tag{A.1}$$

where: η and λ are ripple height and ripple length respectively (Appendix B); the factor μ varies linearly between $\mu = 1$ for sand with $d_{50} \geq 0.2$ mm to $\mu = 6$ for sand with $d_{50} \leq 0.15$ mm and has the effect of higher bed roughness for fine-sand sheet flow conditions caused by large sheet-flow layer thickness:

$$\mu = \begin{cases} 6 & \text{if } d_{50} \leq 0.15\text{mm} \\ 6 - \dfrac{5(d_{50} - 0.15)}{(0.20 - 0.15)} & \text{if } 0.15\text{mm} < d_{50} < 0.20\text{mm} \\ 1 & \text{if } d_{50} \geq 0.20\text{mm} \end{cases} \tag{A.2}$$

in which d_{50} is entered in mm, $\langle|\theta|\rangle$ is the time-averaged absolute Shields stress given by:

$$\langle|\theta|\rangle = \frac{\frac{1}{2} f_\delta |u_\delta|^2}{(s-1) g d_{50}} + \frac{\frac{1}{4} f_w \hat{u}^2}{(s-1) g d_{50}} \tag{A.3}$$

where f_w is the full-cycle wave friction factor based on Swart (1974):

$$\begin{aligned} f_w &= 0.00251 \exp\left[5.21\left(\frac{\hat{a}}{k_{sw}}\right)^{-0.19}\right] && \text{for} \quad \frac{\hat{a}}{k_{sw}} > 1.587 \\ f_w &= 0.3 && \text{for} \quad \frac{\hat{a}}{k_{sw}} \leq 1.587 \end{aligned} \tag{A.4}$$

The wave-related bed roughness k_{sw} is given by :

$$k_{sw} = \max\{d_{50}, d_{50}[\mu + 6(\langle|\theta|\rangle - 1)]\} + 0.4\eta^2 / \lambda \tag{A.5}$$

Here a lower grain size related limit of $k_{sw} = d_{50}$ (instead of $3d_{90}$ as per Eq. (A.1)) gave best results similar to Ribberink (1998). In the case of sheet flow conditions, the bed roughness needs to be solved iteratively because the mean absolute Shields parameter $\langle|\theta|\rangle$ depends on the bed roughness.

APPENDIX B: *Ripple dimensions*

In applications where the ripple dimensions are unknown, the ripple predictor of O'Donoghue et al. (2006) is incorporated:

$$\frac{\eta}{\hat{a}} = m_\eta n_\eta \left(0.275 - 0.022\hat{\psi}^{0.42}\right) \tag{B.1}$$

$$\frac{\lambda}{\hat{a}} = m_\lambda n_\lambda \left(1.97 - 0.44\hat{\psi}^{0.21}\right) \tag{B.2}$$

where:

$$m_\eta = \begin{cases} 0.55 & \text{if } d_{50} \le 0.22\,\text{mm} \\ 0.55 + \dfrac{0.45\left(d_{50} - 0.22\right)}{\left(0.30 - 022\right)} & \text{if } 0.22\,\text{mm} \le d_{50} < 0.30\,\text{mm} \\ 1 & \text{if } d_{50} \ge 0.30\,\text{mm} \end{cases} \tag{B.3}$$

$$m_\lambda = \begin{cases} 0.73 & \text{if } d_{50} \le 0.22\,\text{mm} \\ 0.73 + \dfrac{0.27\left(d_{50} - 0.22\right)}{\left(0.30 - 022\right)} & \text{if } 0.22\,\text{mm} \le d_{50} < 0.30\,\text{mm} \\ 1 & \text{if } d_{50} \ge 0.30\,\text{mm} \end{cases} \tag{B.4}$$

with $\hat{\psi} = \max(\hat{\psi}_c, \hat{\psi}_t)$ for regular flow, whereby the maximum mobility number at crest or trough is defined as $\hat{\psi}_i = \hat{u}_i^2/(s-1)gd_{50}$, and for irregular flow $\hat{\psi} = \hat{\psi}_{1/10} = \hat{u}_{1/10}^2/(s-1)gd_{50}$. Since information on $\hat{u}_{1/10}$ (average of the highest one-tenth orbital velocities) is not available for most irregular flow datasets, it is for simplicity assumed that the irregular flows are Rayleigh distributed, therefore $\hat{u}_{1/10} = 1.27\hat{u}$.

To avoid strong discontinuities in the predicted net transport rates with increasing flow intensities, the factors n_η and n_λ are introduced to allow for a smooth transition between the ripple regime and the flat bed sheet flow regime:

$$n_\eta = n_\lambda = \begin{cases} 1 & \text{if } \hat{\psi} \le 190 \\ \dfrac{1}{2}\left(1 + \cos\left\{\pi \dfrac{\left(\hat{\psi} - 190\right)}{\left(240 - 190\right)}\right\}\right) & \text{if } 190 < \hat{\psi} < 240 \\ 0 & \text{if } \hat{\psi} \ge 240 \end{cases} \tag{B.5}$$

APPENDIX C: *Sheet-flow layer thickness*

The sheet flow layer thickness δ_{si} is calculated following Dohmen-Janssen (1999):

$$\frac{\delta_{si}}{d_{50}} = \begin{cases} 25\hat{\theta}_i & \text{if } d_{50} \le 0.15 \text{ mm} \\ \left[25 - \dfrac{12\left(d_{50} - 0.15\right)}{\left(0.20 - 0.15\right)}\right]\hat{\theta}_i & \text{if } 0.15 \text{ mm} < d_{50} < 0.20 \text{ mm} \\ 13\hat{\theta}_i & \text{if } d_{50} \ge 0.20 \text{ mm} \end{cases} \tag{C.1}$$

where $\hat{\theta}_i$ is Shields parameter based on the crest/trough velocity amplitude $\hat{u}_i$ as follows:

$$\hat{\theta}_i = \frac{\frac{1}{2} f_{w\delta i} \hat{u}_i^{\,2}}{(s-1) g d_{50}} \tag{C.2}$$

with $f_{w\delta i}$ the wave-current friction factor according Eq. (18) and wave and current related roughness as detailed in Appendix A. For fine sand ($d_{50} \le 0.15$mm) Eq. (C.1) differs slightly from Dohmen-Janssen's (1999) original equation since the constant is recalibrated (here 25 instead of 35 in the original) as a result of the increase in the wave related roughness for fine sands (see Section 3.3).

APPENDIX D: *Adjustment time scale of sediment concentration under progressive surface waves*

For the adjustment time scale T_A for the concentration of sediment under progressive surface waves, we follow the parameterization recently proposed by Kranenburg et al. (in press). An expression for T_A has been derived from the (turbulence-averaged) advection-diffusion equation for sediment concentration:

$$\frac{\partial C}{\partial t} + \frac{\partial uC}{\partial x} = \frac{\partial \left(w_s - w\right) C}{\partial z} + \frac{\partial}{\partial z}\left(\varepsilon \frac{\partial C}{\partial z}\right) \tag{D.1}$$

where C is the sand volume concentration, ε is the turbulent mixing coefficient. The equation describes how horizontal and vertical advection (including settling of sediment) and vertical turbulent diffusion lead to temporal concentration adjustment. This includes the time-dependent entrainment and deposition of sediment from and to the bed and the lagging of sand

concentration in the wave boundary layer behind the time-dependent bed shear stress (phase-lag effects).

For horizontal oscillatory flow (w = 0, uniform flow: $\partial../\partial x = 0$) this equation reduces to:

$$\frac{\partial C}{\partial t} = \frac{\partial w_s C}{\partial z} + \frac{\partial}{\partial z}\left(\varepsilon \frac{\partial C}{\partial z} \right) \tag{D.2}$$

This advection-diffusion model was recently applied successfully for tunnel flows for various grain sizes and a range of sheet flow conditions (Ruessink et al., 2009; Hassan and Ribberink, 2010). For uniform surface waves propagating over a horizontal bed, the non-uniformity in x can be transformed to a time-dependency using $\frac{\partial..}{\partial x} = -\frac{1}{c_w}\frac{\partial..}{\partial t}$. Eq. (D.1) can now be rewritten as:

$$\left(1 - \frac{u}{c_w}\right)\frac{\partial C}{\partial t} = \frac{\partial}{\partial z}\left((w_s - w)C + \varepsilon \frac{\partial C}{\partial z} \right) = \frac{\partial}{\partial z}(\phi_{\text{vert}}) \tag{D.3}$$

Herein the factor (1-u/c_w) represents the influence of horizontal sediment advection. The right hand side of Eq. (D.3) represents (the vertical gradient of) the vertical sediment flux ϕ_{vert} due to vertical advection and turbulent diffusion.

Following the method of Galappatti and Vreugdenhil (1985) for shallow, gradually varying flows, we approximate the advection-diffusion Eq. (D.3) by a relaxation equation for the depth-averaged sediment concentration $\bar{C}$. The depth-averaging is carried out over the maximum thickness Δ of the sediment flux layer in the wave boundary layer:

$$\frac{\partial \bar{C}}{\partial t} = \frac{\gamma\left(\bar{C}_{\text{eq}} - \bar{C}\right)}{T_{\text{A}}} \tag{D.4}$$

In this relaxation equation T_{A} is the adjustment time of the actual sediment concentration, which lags behind its equilibrium value $\bar{C}_{\text{eq}}$, as imposed by the instantaneous bed shear stress (the phase-lag effect). The adjustment time is different for oscillatory flows and for progressive surface waves:

$$T_A = \frac{\Delta}{w_s}\left(1 - \frac{\xi u_w}{c_w}\right) \qquad \text{progressive surface waves} \qquad \text{(D.5)}$$

$$T_A = \frac{\Delta}{w_s} \qquad \text{oscillatory tunnel flows} \qquad \text{(D.6)}$$

Herein ($1\text{-}u_w / c_w$) expresses the influence of horizontal advection, in which the velocity u_w is the time-dependent free stream orbital velocity. The coefficient γ and ξ are shape coefficients related to the shape of the velocity and concentration profiles. Here we relate Δ to the representative sediment stirring height, which in the sheet flow regime is the sheet flow layer thickness or the ripple height in case of rippled beds.

REFERENCES

Apsley, D.D., Stansby, P.K., 2008. Bed-load sediment transport on large slopes: model formulation and implementation within a RANS solver. *Journal of Hydraulic Engineering*, 134(10), 1440-1451.

Bailard, J.A., 1981. An energetics total load sediment transport model for a plane sloping beach. *Journal of Geophysical Research*, 86(C11), 10938-10954.

Bijker, E.W., 1971. Longshore transport computations. *J. Waterway, Port, Coastal and Ocean Engineering*, 97, 687-701.

Butt, T., Russell, P., Puleo, J., Miles, J., Masselink, G., 2004. The influence of bore turbulence on sediment transport in the swash and inner surf zones. *Continental Shelf Research*, 24, 757 – 771.

Camenen, B., Larson, M., 2007. A total load formula for the nearshore. *Proc. Coastal Sediments '07*. ASCE, New Orleans, Louisiana, USA.

Clubb, G.S., 2001. Experimental study of vortex ripples in full scale sinusoidal and asymmetric flows. PhD thesis, University of Aberdeen, UK.

Day, T.J., 1980. A study of transport of graded sediments. Report no. IT 190, Hydraulics Research Station, Wallingford, UK.

Deigaard, R., Fredsøe, J., Broker-Hedegaard, I., 1986. Suspended sediment in the surf zone. ASCE, *Journal of Waterway Port Coastal and Ocean Engineering*, 112(1), 115-128.

Dibajnia, M., Watanabe, A., 1992. Sheet flow under non linear waves and currents. *Proceedings 23rd International Conference on Coastal Engineering*, ASCE, 2015-2028.

Dibajnia, M., Watanabe, A., 1996. A transport rate formula for mixed sands. *Proceedings 25th International Conference on Coastal Engineering*, ASCE, 3791-3804.

Dibajnia, M., Watanabe, A., 1998. Transport rate under irregular sheet flow conditions. *Coastal Engineering*, 35, 167-183.

Dibajnia, M., Kioka, W., 2000. Long waves and the change in cross-shore sediment transport rates on a sheet flow dominated beach. *Coastal Engineering Japan*, 42(1), 87-110.

Dibajnia, M., Moriya, T., Watanabe, A., 2001. A representative wave model for estimation of nearshore local transport rate. *Coastal Engineering Japan*, 43(1), 1-38.

Dohmen-Janssen, C.M., 1999. Grain size influence on sediment transport in oscillatory sheet flow, phase lags and mobile-bed effects, Ph.D. thesis, Delft University of Technology, The Netherlands.

Dohmen-Janssen, C.M., Kroekenstoel, D.F., Hassan, W.N., Ribberink, J.S., 2002. Phase lags in oscillatory sheet flow: experiments and bed load modelling. *Coastal Engineering*, 46, 61-87.

Dohmen-Janssen, C.M., Hanes, D.M., 2002. Sheet flow dynamics under monochromatic nonbreaking waves. *Journal Geophysical Research*, 107(C10), 3149.

Fredsøe, J., Deigaard, R., 1992. *Mechanics of coastal sediment transport*. Advanced series on Ocean Engineering, vol 3. World Scientific.

Galappatti, R., Vreugdenhil, C.B., 1985. A depth-integrated model for suspended sediment transport. *Journal of Hydraulic Research*, 23(4), 359-377.

Gonzalez-Rodriguez, D., Madsen, O.S., 2007. Seabed shear stress and bedload transport due to asymmetric and skewed waves. *Coastal Engineering*, 54, 914-929.

Grant, W.D., Madsen, O.S., 1982. Moveable bed roughness in oscillatory flow. *Journal of Geophysical Research*, 87(C1), 469-481.

Guy, H.P., Simons, D.B., Richardson., E.V., 1966. Summary of alluvial channel data from flume experiments 1956-1961, US Geological Survey, Prof. Paper 462-I, Washington, DC.

Hamm, L., Katapodi, I., Dohmen-Janssen, M., Ribberink, J.S., Samothrakis, P., Cloin, B., Savioli, J.C., Chatelus, Y., Bosboom, J., Nicholson, J., Hein, R., 1998. Grain size, gradation and density effects on sediment transport processes in oscillatory flow conditions. Data report, Part I.WL|Delft Hydraulics, the Netherlands.

Hassan,W.N.M., 2003. Transport of size-graded and uniform sediments under oscillatory sheet-flow conditions. PhD thesis, University of Twente, the Netherlands.

Hassan, W.N.M., Ribberink, J.S., 2010. Modelling of sand transport under wave-generated sheet flows with a RANS diffusion model. *Coastal Engineering*, 57(1), 19-29.

Henderson, S.M., Allen, J.S., Newberger, P.A., 2004. Nearshore sandbar migration predicted by an eddy-diffusive boundary layer model. *Journal of Geophysical Research*, 109, C06024, doi:10.1029/2003JC002137.

Holmedal, L.E., Myrhaug, D., 2009. Wave-induced steady streaming, mass transport and net sediment transport in rough turbulent ocean bottom boundary layers. *Continental Shelf Research*, 29, 911-926.

Humbyrd, C.J., Madsen, O.S., 2011. Predicting movable bed roughness in coastal waters. *Proceedings of International Conference on Coastal Engineering*, No. 32(2010), Shanghai, China. Paper #:sediment.6.

Inui, T., Dibajnia, M., Isobe, M.,Watanabe, A., 1995. A transport rate formula for mixed-size sands and its application. *Proceedings 42nd Japanese Annual Conference on Coastal Engineering*, pp. 356–360 (in Japanese).

Katapodi, I., Ribberink, J.S., Ruol, P., Koelewijn, R., Lodahl, C., Longo, S., Crosato, A., Wallace, H., 1994. Intra-wave sediment transport in oscillatory flow superimposed on a mean current. Data report, Part III. WL|Delft Hydraulics, the Netherlands.

Kobayashi, N., Johnson, B.D., 2001. Sand suspension, storage, advection, and settling in surf and swash zones. *Journal of Geophysical Research,* 106(C5), 9363-9376.

Kranenburg, W.M., Ribberink, J.S., Schretlen, J.J.L.M., Uittenbogaard, R.E., (in press). Sand transport beneath waves: the role of progressive wave streaming and other free surface effects. *Journal of Geophysical Research.*

Longuet-Higgins, M.S., 1953. Mass transport in water waves. *Phil. Trans. R. Soc. Lon. A.*, 245, 535-581.

Longuet-Higgins, M.S., 1958. The mechanics of the boundary-layer near the bottom in a progressive wave. *Proceedings 6th International Conference on Coastal Engineering*, ASCE, 184-193.

Madsen, O.S., Grant, W.D., 1976. Sediment transport in the coastal environment. MIT Ralph M. Parsons Lab., Rep. 209, Cambridge, USA.

Malarkey, J., Davies, A.G., 2012. Free-stream velocity descriptions under waves with skewness and asymmetry. *Coastal Engineering*, 68, 78-95.

Nielsen, P., 1983. Analytical determination of nearshore wave height variation due to refraction shoaling and friction. *Coastal Engineering*, 7, 223-251.

Nielsen, P., 1988. Three simple models of wave sediment transport. *Coastal Engineering*, 12, 43-62.

Nielsen, P., 2006. Sheet flow sediment transport under waves with acceleration skewness and boundary layer streaming. *Coastal Engineering*, 53, 749-758.

Nnadi, F.N., Wilson, K.C., 1992. Motion of contact-load particles at high shear stress. *Journal of Hydraulic Engineering*, 118(12), 1670-1684.

O'Donoghue, T., Wright, S. 2004. Concentrations in oscillatory sheet flow for well sorted and graded sands. *Coastal Engineering*, 50, 117-138.

O'Donoghue, T., Doucette, J.S., van der Werf, J.J., Ribberink, J.S., 2006. The dimensions of sand ripple in full-scale oscillatory flows. *Coastal Engineering*, 53, 997-1012.

Ramadan, K.A.H., 1994. Time-averaged sediment transport phenomena in combined wave-current flow. Report H 1889.11, Part I. WL|Delft Hydraulics, the Netherlands.

Raudkivi, A.J., 1988. The roughness height under waves. *Journal of Hydraulic Research*, 26(5), 569-584.

Ribberink, J.S., 1995. Time-averaged sediment transport phenomena in combined wave-current flow. Report H 1889.11, Part II. WL|Delft Hydraulics, the Netherlands.

Ribberink, J.S., 1998. Bed-load transport for steady flows and unsteady oscillatory flows. *Coastal Engineering*, 34, 59-82.

Ribberink, J.S., Chen, Z., 1993. Sediment transport of fine sand under asymmetric oscillatory flow. Data report H 840.20, Part VII.WL|Delft Hydraulics, the Netherlands.

Ribberink, J.S., Al-Salem, A.A.,1994. Sediment transport in oscillatory boundary layers in cases of rippled beds and sheet flow. *Journal of Geophysical Research*, 99 (C6), 12,707–12,727.

Ribberink, J.S., Al-Salem, A.A., 1995. Sheet flow and suspension of sand in oscillatory boundary layers. *Coastal Engineering*, 25, 205–225.

Ribberink, J.S., Dohmen-Janssen, C.M., Hanes, D.M., McLean, S.R., Vincent, C., 2000. Near-bed sand transport mechanisms under waves. *Proceedings 27th International Conference on Coastal Engineering*. ASCE, 3263–3276.

Roelvink, J.A., Stive, M.J.F., 1989. Bar-generating cross-shore flow mechanisms on a beach. *Journal of Geophysical Research*, 94(C4), 4785 – 4800.

Ruessink, B.G., van den Berg, T.J.J., van Rijn, L.C. 2009. Modeling sediment transport beneath skewed asymmetric waves above a plane bed. *Journal of Geophysical Research*, 114, C11021, doi:10.1029/2009JC005416.

Ruessink, B.G., Michallet, H., Abreu, T., Sancho, F., van der A, D.A., Van der Werf, J.J., Silva, P.A., 2011. Observations of velocities, sand concentrations, and fluxes under velocity-asymmetric oscillatory flows. *Journal of Geophysical Research*, 116, C03004, doi:10.1029/2010JC006443.

Ruessink, B.G., Ramaekers, G., van Rijn, L.C., 2012. On the parameterization of the free-stream non-linear wave orbital motion in nearshore morphodynamic models. *Coastal Engineering*, 65, 56-63.

Sato, S., 1987. Oscillatory boundary layer flow and sand movement over ripples. PhD thesis, University of Tokyo, Japan.

Schretlen, J.J.L.M., Ribberink, J.S., O'Donoghue, T., 2011. Boundary layer flow and sand transport under full scale surface waves. *Proceedings of the International Conference on Coastal Engineering*, No. 32(2010), Shanghai, China. Paper #: sediment.4.

Silva, P.S., Temperville, A. Seabra Santos, F., 2006. Sand transport under combined current and wave conditions: A semi-unsteady, practical model. *Coastal Engineering*, 53, 897-913.

Silva, P.S., Abreu, T., van der A, D.A., Sancho, F., Ruessink, B.G., van der Werf, J.J., Ribberink, J.S., 2011. Sediment transport in nonlinear skewed oscillatory flows: Transkew experiments. *Journal of Hydraulic Research*, 49(S1), 72-80.

Sleath, J.F.A., 1987. Turbulent oscillatory flow over rough beds. *Journal of Fluid Mechanics*, 182, 369-409.

Soulsby, R.L., 1997. *Dynamics of Marine Sands*. Thomas Telford Publications, London.

Soulsby, R.L., Damgaard, J.S., 2005. Bedload sediment transport in coastal water. *Coastal Engineering*, 52, 673-689.

Soulsby, R.L., Whitehouse, R.J.S., Marten, K.V., 2012. Prediction of time-evolving sand ripples in shelf seas. *Continental Shelf Research*, 38, 47-62.

Suntoyo, Tanaka, H. Sana, A., 2008. Characteristics of turbulent boundary layers over a rough bed under saw-tooth waves and its application to sediment transport. *Coastal Engineering*, 55, 1102-1112.

Swart, D.H., 1974. Offshore sediment transport and equilibrium beach profiles. Delft Hydr. Lab. Publ., No.131, Delft Hydraulics, The Netherlands.

Swart, D.H., 1976. Predictive equations regarding coastal transports. *Proceedings 15th Conference on Coastal Engineering*, ASCE, 1113-1132.

Van den Berg, J.H., 1986. Aspects of sediment and morphodyanmics of subtidal deposits of the Oosterscehlde (the Netherlands), Rijkswaterstaat, Communications no. 43.

Van der A, D.A., O'Donoghue, T., Ribberink, J.S. 2009. Sheet flow sand transport processes in oscillatory flow with acceleration skewness, paper 133, *Proceedings Coastal Dynamics'09*, World Scientific.

Van der A, D.A., O'Donoghue, T., Ribberink, J.S. 2010. Measurements of sheet flow transport in acceleration-skewed oscillatory flow and comparison with practical formulations. *Coastal Engineering*, 57, 331-342.

Van der A, D.A., O'Donoghue, T., Davies, A.G., Ribberink, J.S., 2011. Experimental study of the turbulent boundary layer in acceleration-skewed oscillatory flow. *Journal of Fluid Mechanics*, 684, 251-283.

Van der Werf, J.J., Ribberink, J.S., O'Donoghue, T., Doucette, J.S., 2006. Modelling and measurement of sand transport processes over full-scale ripples in oscillatory flows. *Coastal Engineering*, 53, 657–673.

Van der Werf, J.J., Doucette, J.S., O'Donoghue, T., Ribberink, J.S., 2007. Detailed measurements of velocities and suspended sand concentrations over full-scale ripples in regular oscillatory flow. *Journal of Geophysical Research,* 112, F02012.

Van der Werf, J.J., Schretlen, J.J.L.M., Ribberink, J.S., O'Donoghue, T., 2009. Database of full-scale laboratory experiments on wave-driven sand transport processes. *Coastal Engineering*, 56, 726-732.

Van der Werf, J.J., Nomden, H., Ribberink, J.S., Walstra, D.J.R., Kranenburg, W.M., 2012. Application of a new sand transport formula within the cross-shore morphodynamic model UNIBEST-TC. *Coastal Engineering Proceedings*, 1(33), sediment.5.

Van Rijn, L. C., 1993. *Principles of sediment transport in rivers, estuaries and coastal seas*, Aqua Publications, Amsterdam, The Netherlands.

Van Rijn, L.C., 2007a. Unified view of sediment transport by currents and waves. I: Initiation of motion, bed roughness, and bed load transport. *Journal of Hydraulic Engineering*, 133(6), 649-667.

Van Rijn, L.C., 2007b. Unified view of sediment transport by currents and waves. II: Suspended Transport. *Journal of Hydraulic Engineering*, 133(6), 668-689.

Van Rijn, L.C., 2007c. Unified view of sediment transport by currents and waves. III: Graded Beds. *Journal of Hydraulic Engineering*, 133(7), 761-775.

Van Rijn, L.C., Walstra, D.J.R., Grasmeijer, B., Sutherland, J., Pan, S., Sierra, J.P., 2003. The predictability of cross-shore bed evolution of sandy beaches at the time scale of storms and season using process-based Profile models. *Coastal Engineering*, 47, 295–327.

Vincent, C.E., Hanes, D.M., 2002. The accumulation and decay of nearbed suspended sand concentration due to waves and wave groups. *Continental Shelf Research*, 22, 1987 - 2000.

Wang, Y.-H., 2007. Formula for predicting bedload transport rate in oscillatory sheet flows. *Coastal Engineering*, 54, 594-601.

Watanabe, A., Sato, S., 2004. A sheet-flow transport rate formula for asymmetric forward-leaning waves and currents. *Proceedings 29th International Conference on Coastal Engineering*. World Scientific, 1703–1714.

Wright, S., O'Donoghue, T., 2002. Total sediment transport rate predictions in wave current sheet flow with graded sand. Oscillatory Flow Tunnel Experiments at Aberdeen University, Experimental Report EPSRC LUBA Project. University of Aberdeen, UK.

Zyserman, J.A., Fredsøe, J., 1994. Data analysis of bed concentration of suspended sediment. *Journal of Hydraulic Engineering*, 120, 1021-1042.

TABLES

Flow condition	d_{50}	$T_{(p)}$	$u_{w,\max(sig)}$	u_δ	$\Psi_{\max(sig)}$	$\beta_{(sig)}$	$R_{(sig)}$	Number of conditions					Reference(s)
	(mm)	(s)	(m/s)	(m/s)	(-)	(-)	(-)	reg.	irreg.	s.f.	rip.	total	
sinusoidal osc. flows	0.22	10.2	0.63	–	79	0.5	0.5	–	1	–	1	1	Van der Werf et al. (2006)
velocity-skewed osc. flows	0.13–0.46	4–12.5	0.16–1.72	–	9–1427	0.5	0.52–0.70	70	22	40	52	92	Sato (1987); Dibajnia and Watanabe (1992); Ribberink and Chen (1993); Ribberink and Al-Salem (1994); Ribberink and Al-Salem (1995); Clubb (2001); Wright and O'Donoghue (2002); Hassan (2003); O'Donoghue and Wright (2004); Van der Werf et al. (2006); Van der Werf et al. (2007); Silva et al. (2011)
acceleration-skewed osc. flows	0.15–0.46	5–10	0.83–1.45	–	225–702	0.56–0.8	0.5	–	–	47	–	47	Watanabe and Sato (2004); Van der A et al. (2010); Silva et al. (2011)
acceleration + velocity skewed osc. flows	0.15; 0.20	7–10	0.94–1.61	–	364–793	0.60–0.72	0.53–0.60	6	–	6	–	6	Van der A et al. (2010); Silva et al. (2011)
oscillatory flows with current	0.13–0.32	4–12	0.94–1.69	-0.50 – 0.50	269–841	0.5–0.7	0.5–0.70	50	–	50	–	50	Dibajnia and Watanabe (1992); Katapodi et al. (1994); Ramadan (1994); Dohmen-Janssen (1999); Silva et al. (2011)
graded sands	0.15–0.54	5–12	0.72–1.63	0.24; 0.45		0.50	0.5–0.68	19	–	19	–	19	Iniu et al. (1995); Hamm et al. (1998); Hassan (2003); O'Donoghue and Wright (2004)
progressive surface waves	0.14–0.25	5–9.1	1.02–1.66	–	270–1079	0.46–0.56	0.55–0.67	11	–	11	–	11	Dohmen-Janssen and Hanes (2002); Schretlen et al. (2011)
Total	0.13–0.54	4 – 12.5	0.16–1.72	-0.50–0.50	9–1427	0.46–0.8	0.5–0.70	203	23	173	53	226	

Table 1. Overview of dataset used for development and calibration of the formula. The number of conditions is divided per flow (regular, irregular) and per transport regime (sheet flow, rippled bed). Here d_{50} is the median grain diameter, $T_{(p)}$ the (peak) flow period, $u_{w,\max}$ the maximum orbital velocity, u_δ the net current velocity (negative indicates a current direction opposite that of the implied wave direction) at level $z = \delta$ computed from the measured or imposed current velocity by assuming a logarithmic velocity profile with δ = 0.2m, $\Psi_{\max}$ is the mobility number based on $u_{w,\max}$, and β and R represent the degree of velocity and acceleration skewness, respectively (see Section 2.1). The subscript (*sig*) applies to the irregular flow conditions for which significant (i.e. average of the highest one-third) values are listed.

Data (sub)set	*N*	*BSS*	*bias (%)*	r^2	fac2 (%)	fac5 (%)
Velocity-skewed sheet flow $d_{50} \geq 0.20$mm	32	0.91	-8	0.78	97	100
Acceleration-skewed sheet flow $d_{50} \geq 0.20$mm	32	0.92	2	0.87	84	97
Oscillatory sheet flow $d_{50} < 0.20$mm	29	0.73	-8	0.80	86	93
Oscillatory flow over rippled beds	53	0.72	4	0.65	62	89
Oscillatory flow with collinear current	50	0.72	61	0.84	70	86
Graded sands	19	0.83	45	0.91	89	100
Progressive surface waves	11	0.57	27	-1.05	82	100
Regular flows	203	0.76	18	0.76	81	94
Irregular flows	23	0.54	18	0.95	57	87
Sheet flow	173	0.76	22	0.73	83	94
Ripples	53	0.72	4	0.65	62	89
Fine sand ($d_{50} < 0.20$mm)	64	0.70	-16	0.72	77	89
Coarse sand ($d_{50} \geq 0.20$mm)	162	0.79	31	0.85	79	94
All	226	0.76	18	0.77	78	93
All with ripple predictor	226	0.76	10	0.76	69	86

Table 2. Performance criteria for the various data subsets. *N* indicates the number of data points contained in the subset, *BSS* is the Brier Skill Score (Van Rijn et al., 2003; Van der A et al., 2010), here $BSS = 1 - \left\langle \left| q_{s,pred} - q_{s,meas} \right|^2 \right\rangle / \left\langle q_{s,meas}^2 \right\rangle$ which gives a measure of the formula accuracy (*BSS* = 1 means perfect agreement, BSS < 0 means that the transport rate error is greater than when zero transport is predicted for each condition, i.e. the "do-nothing" scenario), *bias* is the normalized mean bias defined as $bias = \left\langle \left(q_{s,pred} - q_{s,meas} \right) / q_{s,meas} \right\rangle$ and indicates the tendency of the formula to over- (positive bias) or underestimate (negative bias) the measurements, r^2 is the squared coefficient of correlation, and the last two columns indicate the percentage of the predictions within a factor 2 and 5 of the measurements. Van Rijn et al. (2003) proposed the following skill qualification: excellent: *BSS* = 1.0–0.8; good: 0.8–0.6; fair: 0.6–0.3; poor: 0.3–0; bad: < 0.

Reference	N	mixture d_{10} (mm)	d_{50} (mm)	d_{90} (mm)	fractions d_1 (mm)	p_1 (%)	d_2 (mm)	p_2 (%)	d_3 (mm)	p_3 (%)
Inui et al. (1995)	1	n/a	0.535	n/a	0.200	50	0.870	50	-	-
Hamm et al. (1998)	2	0.097	0.194	0.406	0.128	50	0.317	50	-	-
Hassan (2003)	3	0.160	0.240	0.990	0.210	70	0.970	30	-	-
	5	0.110	0.150	1.080	0.130	60	0.340	20	0.970	20
O'Donoghue and	2	0.100	0.150	0.400	0.150	60	0.280	30	0.510	10
Wright (2004)	2	0.120	0.270	0.470	0.150	20	0.280	60	0.510	20
	2	0.100	0.260	0.530	0.150	50	0.510	50	-	-

Table 3. Sand size characteristics for the graded sand conditions. The d_{10}, d_{50} and d_{90} grain diameters represent the characteristics of the overall mixture. d_j and p_j indicate the diameter and fraction of the individual uniform sands of which the mixture was composed of.

Reference	d_{50} (mm)	$T_{(sig)}$ (s)	u_{δ} (m/s)	$\Psi_{max(sig)}$ (-)	$\beta_{(sig)}$ (-)	$R_{(sig)}$ (-)	Number of Conditions reg.	irreg.	s.f.	rip.	total
Sato (1987)	0.18	3.68-3.99	-	6-96	0.5	0.52-0.68	-	17	-	17	17
Dibajnia and Watanabe (1998)	0.20	3.6-3.9	+0.06 - +0.16	116-374	0.55-0.61	0.59-0.67	-	17	17	-	17
Dibajnia and Kioka (2000)	0.20	3.6-4.0	-	319-469	0.57-0.63	0.64-0.67	-	12	12	-	12
Dibajnia et al. (2001)	0.55, 0.80	3.6-4.2	-	181-283	0.54-0.58	0.57-0.64	-	12	12	-	12

Table 4. Overview of oscillatory flow conditions used for model validation.

FIGURES

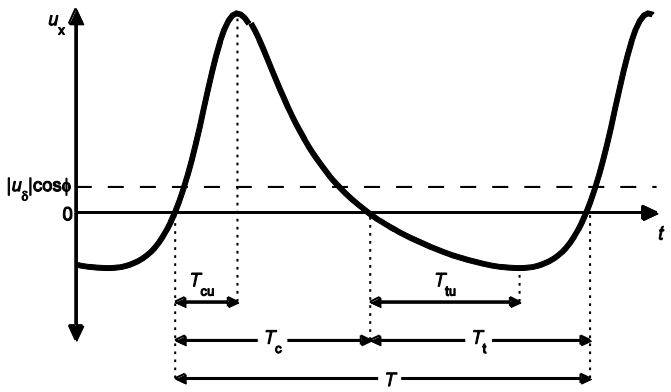

Figure 1. Definition sketch of near-bed velocity time-series in wave direction. The parameters T_c and T_c are the positive (crest) and negative (trough) flow durations. Similarly, T_{cu} and T_{tu} are the durations of flow acceleration in positive and negative *x*-direction.

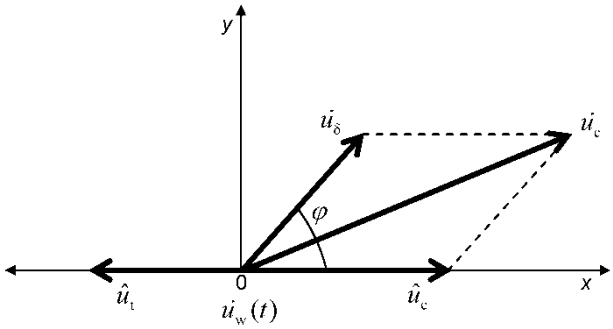

Figure 2. Wave and current velocity vectors $\vec{u}_w(t)$ and $\vec{u}_\delta$ under an angle φ. The vector $\vec{u}_c$ illustrates the resultant velocity vector at maximum positive orbital velocity.

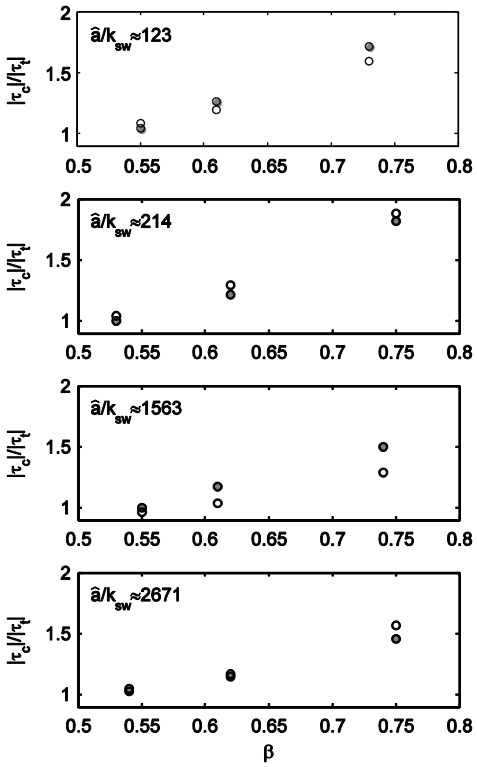

Figure 3. Onshore/offshore bed shear stress ratio as function of β: closed circles: fixed bed measurements of Van der A et al. (2011); open circles: prediction based on Eq. (21) with c_1 = 2.6. Bed shear stress is calculated as $|\tau_i| = 0.5\rho f_{wi}|u_{i,r}|^2$.

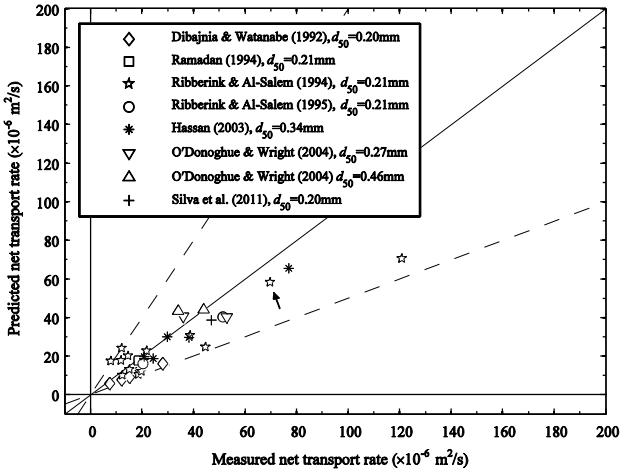

Figure 4. Comparison between measured and calculated net transport rates for velocity-skewed oscillatory sheet flows with $d_{50} \geq 0.20$mm. The solid diagonal indicates perfect agreement, the dashed lines a factor 2 difference.

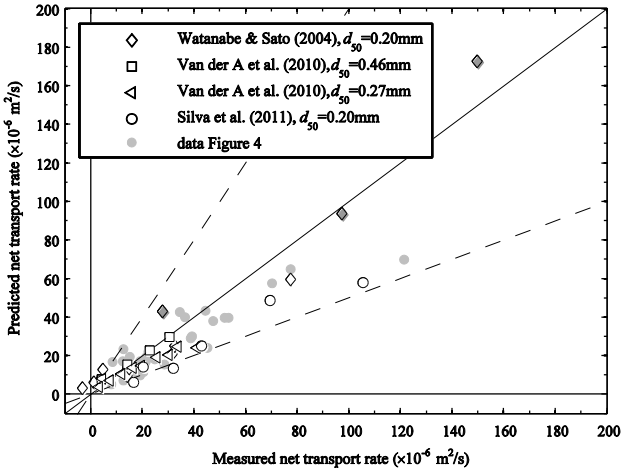

Figure 5. Comparison between measured and calculated net transport rates for acceleration-skewed oscillatory sheet flows with $d_{50} \geq 0.20$mm. The grey diamonds indicate conditions of Watanabe and Sato (2004) for which phase lag effects are active. Note that in Figure 5 toFigure 10**,** data from the preceding figure is included to aid comparison (and is indicated by the small light grey dots).

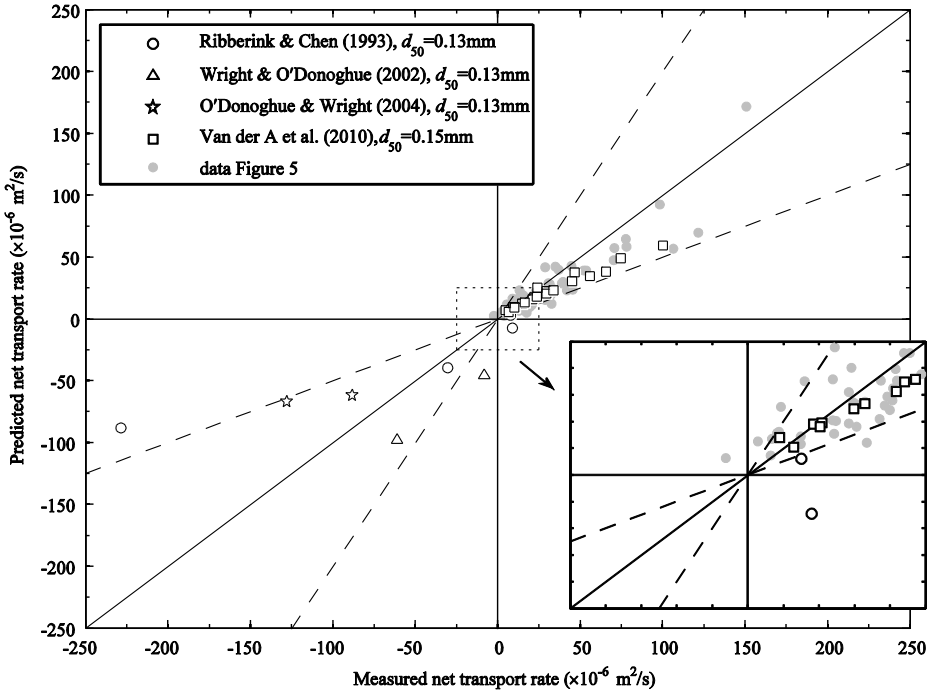

Figure 6. Comparison between measured and calculated net transport rates for oscillatory sheet flows with d_{50} < 0.20mm.

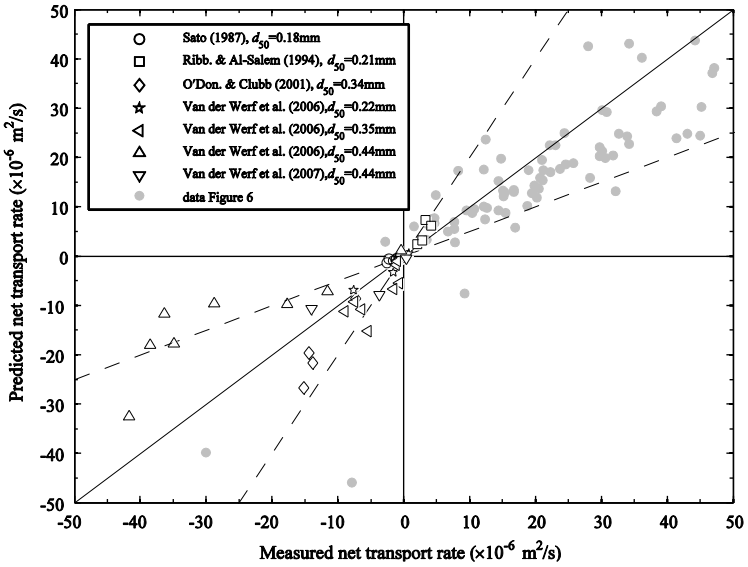

Figure 7. Comparison between measured and predicted net transport rates for oscillatory flows over rippled beds (note the difference in scale between Figure 7. and Figure 6.).

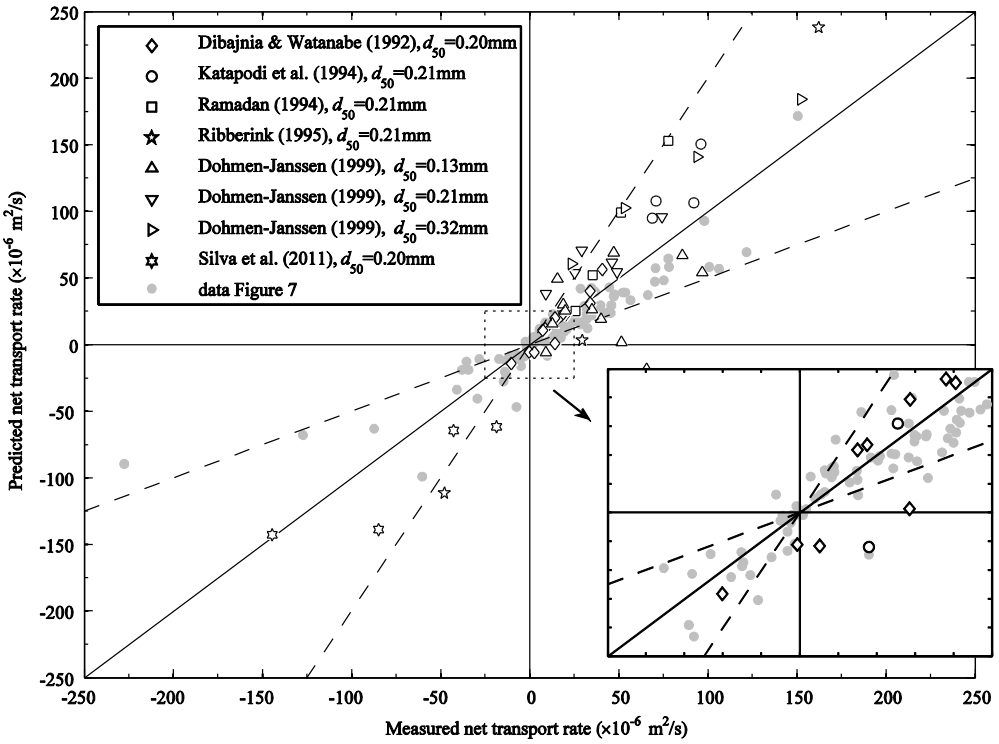

Figure 8. Comparison between measured and predicted net transport rates for oscillatory flows with collinear currents.

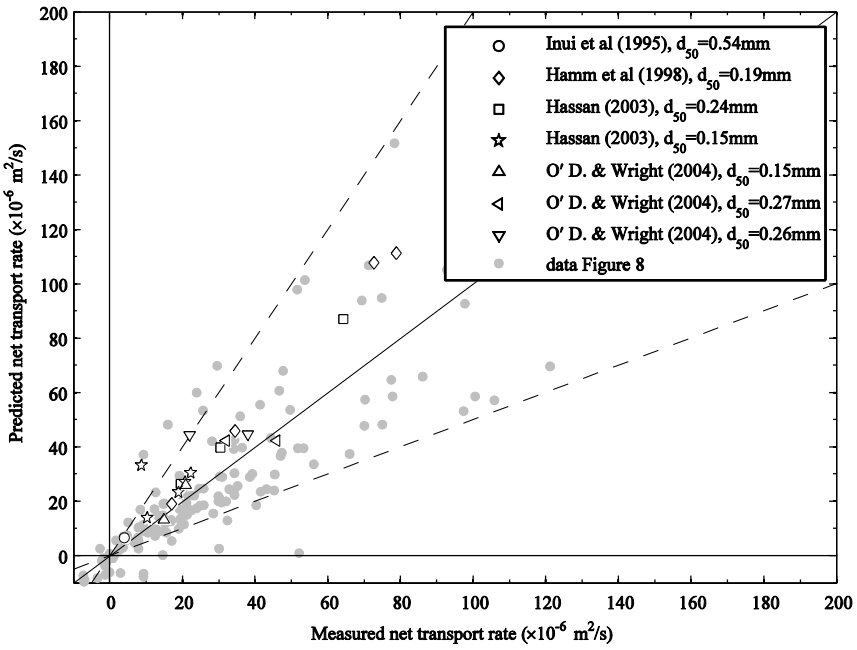

Figure 9. Comparison between measured and predicted net transport rates for graded sand conditions. The value of d_{50} in the legend relates to the overall sand mixture, the characteristics of the individual fractions are listed in Table 3.

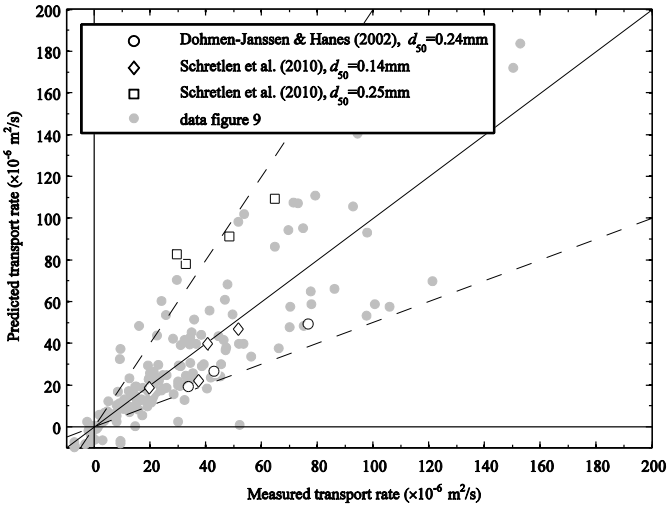

Figure 10. Measured and predicted net transport rates for progressive surface wave conditions.

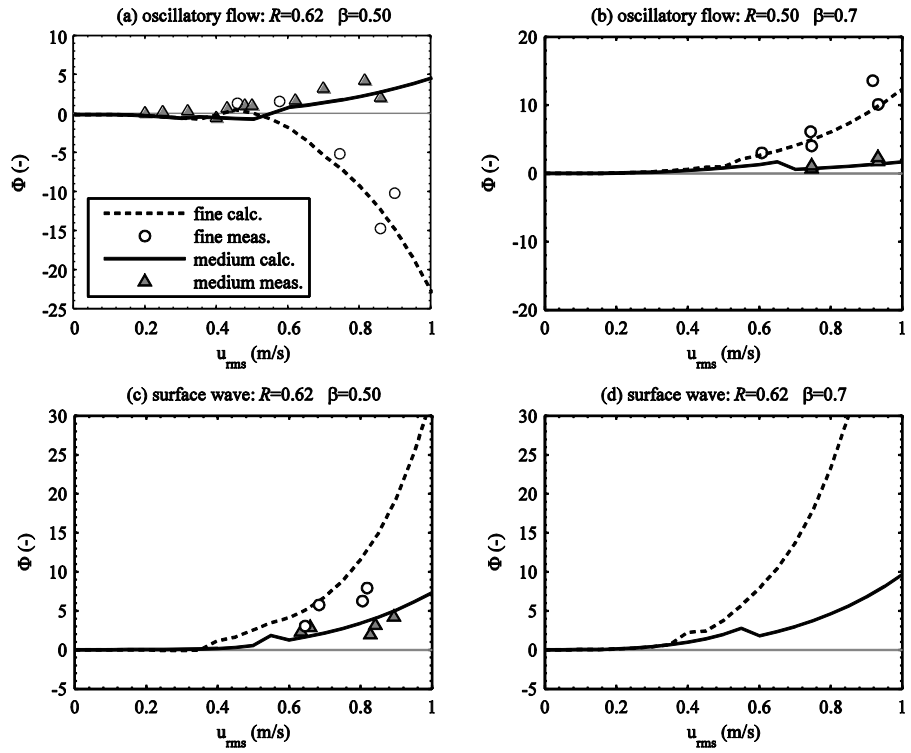

Figure 11. Calculated non-dimensional transport rates against u_{rms} for a fine (d_{50} = 0.13mm) and medium sand (d_{50} = 0.25mm). For all calculated conditions T = 6.5s and for the surface wave conditions (c-d) the water depth is constant with h = 3.5m. The various symbols are experimental results selected from the studies in Table 1 with values of T, R, and β close to the values used for the calculations and sand size d_{50} < 0.20mm for fine sand and medium sand in the range $0.2 \leq d_{50} < 0.30$.

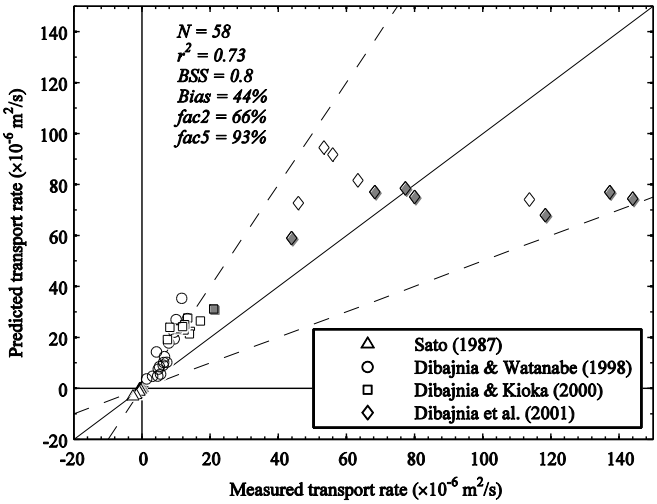

Figure 12. Comparison between measured and calculated net transport rate for oscillatory flows conditions listed in Table 4; grey markers indicate conditions with $T > 4$s.

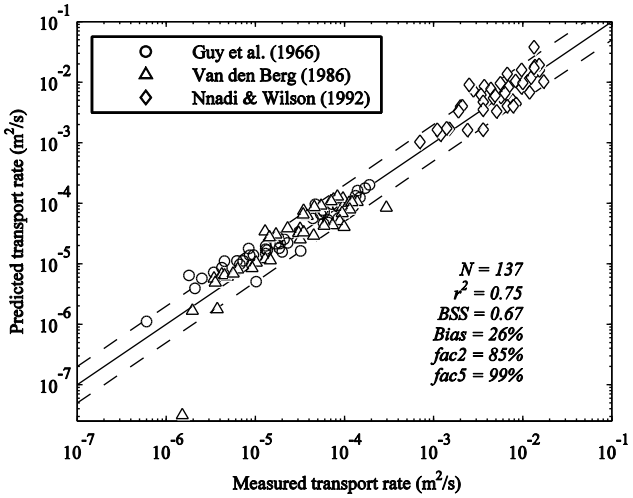

Figure 13. Performance of the formula for steady flow sheet-flow conditions.

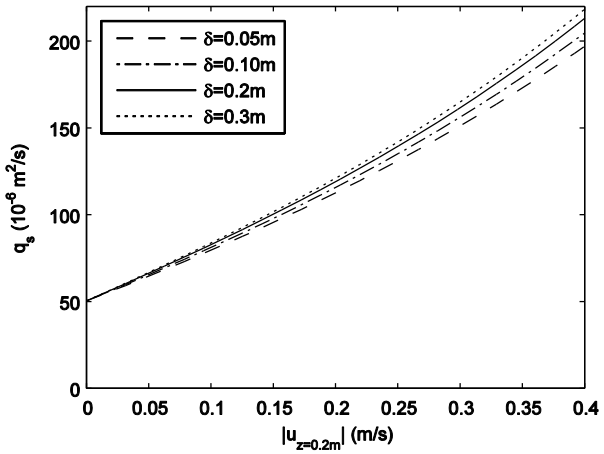

Figure 14. Predicted transport rate as a function of the net current velocity at z = 0.2m for different reference levels δ for the net current within the new formulae. The oscillatory flow condition is a typical sheet flow condition with d_{50} = 0.25 mm, R = 0.625, T = 7.5 s and $\hat{u}$ = 1.25 m/s.